ELSEVIER

Contents lists available at SciVerse ScienceDirect

Precision Engineering

journal homepage: www.elsevier.com/locate/precision



Effect of sampling jitter and control jitter on positioning error in motion control systems

Kristofer Smeds, Xiaodong Lu*

Department of Mechanical Engineering, University of British Columbia, Canada

ARTICLE INFO

Article history:
Received 1 April 2011
Received in revised form 4 August 2011
Accepted 12 September 2011
Available online 4 October 2011

Keywords: Sampling jitter Control jitter Jitter effect Positioning error Motion control

ABSTRACT

In a digital motion control system, there exist timing variations in feedback sampling and control updating, often referred to as sampling jitter and control jitter. Although jitter has been studied in prior art, no equations or quantitative experimental results have been reported which relate jitter to positioning error in a motion control system. To investigate the effect of jitter on positioning error, this paper presents a simplified discrete model that captures sampling and control jitter's interaction with other system inputs as disturbances to the control system. Based on this model, analyses are carried out for the scenarios of position regulation and command tracking, each resulting in an equation to predict jitter's effect on positioning error using measured or analytical frequency responses of the system. Further, an easily implementable add-on jitter compensator is proposed to mitigate the regulation error due to jitter without affecting the existing controller. Through experiments performed on a fast-tool servo machine tool, the model and analyses are validated and the positioning degradation due to jitter is clearly demonstrated

© 2011 Elsevier Inc. All rights reserved.

1. Introduction

In a digital motion control system, there are two periodic events connecting the discrete domain of a digital controller to the continuous domain of the plant to be controlled: a feedback sampling event that samples a sensor feedback signal; and a control updating event that updates the controller's output signal via a zero-orderhold (ZOH). Generally, in digital control system textbooks [1,2] these two events are assumed to happen simultaneously at evenly spaced intervals of sampling period T_0 . In reality, there are several timing problems introduced during the implementation of digital controllers [3]. First, there always exists a delay between the sampling event and the controller output update event due to dataacquisition conversion times and control algorithm computation time. Second, the sampling event intervals are not evenly spaced due to factors such as resource sharing and task scheduling. These sampling event and control event temporal deviations from the ideal timing are referred to as sampling jitter and control jitter,

Usually, sampling jitter and control jitter are assumed small enough to have negligible effects on the closed-loop system performance. Jitter issues have mostly received attention in networked control systems and distributed control systems, in which the

* Corresponding author. E-mail address: XDLU@mech.ubc.ca (X. Lu). sensor node, control calculation node, and actuator node are connected via a network. Networked control can be a cost-effective solution for systems with a large number of sensors and actuators, such as process automation, but such networks may experience large variable delays. Stability and robustness can be a major concern in these systems due to the large magnitudes of random delay and jitter, and thus stability criteria for network controlled system with jitter has been investigated extensively [4–7].

In motion control systems, although networks are widely used for user interface communication and transferring motion trajectory information, the system feedback loop (consisting of sensor data acquisition, control calculation, and actuator update) is highly localized and network is not part of the feedback loop. Therefore, instability caused by sampling jitter and control jitter is rarely an issue in motion control systems.

Measurements have shown that jitter in motion control applications typically ranges from hundreds of nanoseconds to tens of microseconds for commercially available real-time controllers. For example, a modern digital motion controller running real-time Linux has shown several microseconds of jitter [8] and a National Instruments CompactRIO has shown 40 μs of jitter for a 1 kHz control loop [9]. Measurements performed in Appendix A of this paper show the jitter on an xPC Target controller to be 0.81 μs RMS, and the jitter on a dSPACE DS1103 controller to be 0.16 μs RMS. What is of interest is how much this relatively small amount of jitter affects the performance of a motion control system.

To facilitate time-variant analysis and simulation of control systems, Cervin, Lincoln et al. have created True Time [10] and litterbug [11], which are MATLAB based tools that can be used to evaluate a system's sensitivity to delay and jitter [12]. Antunes and Mota presented a True Time simulation of a system with only control jitter and their results showed an increase in positioning error [13]. Zhang et al. have also presented simulation results showing jitter can increase positioning error [14]. There have been very few experimental results reported in literature to actually demonstrate the effect of jitter on motion system performance. One rare example is a motor speed experiment conducted by Kobayashi et al., which compared a case with fixed 0.25 ms sampling period to a case with varying sampling period from 0.25 ms to 0.375 ms [15]. Their results showed a relatively small difference in speed error for these two cases as other error sources appear to dominate the system.

Approximate modeling work has been conducted by Boje to better understand the effect of jitter on a digital control system [16]. He presented an approximate disturbance model in the w-domain for sampling jitter and control jitter by using a Tustin approximation to convert discrete-time controllers to the w-domain. Based on this approximate model he then performed simulations to show jitter caused a disturbance to act on the system.

In order to reduce jitter-induced problems, work has been done in both the areas of real-time computing and control. Developments in real-time computing have focused on task scheduling methods to directly reduce jitter magnitude [17–20]. Work in control has focused on controller design techniques such as H_{∞} and LQG methods to improve system rejection of jitter disturbance [21,22].

Another class of jitter compensators are timestamp-based controllers, which take advantage of runtime timing data (timestamps of actual sampling events) to dynamically compensate for jitter [23–25]. The main limitation of timestamp based controllers is that they introduce additional complexity and overhead into the control task, making them impractical for systems requiring fast sampling rates. Further, timestamps are usually unavailable in many controller hardware implementations, limiting the applicability of this type of solution. Consequently, literature for these proposed methods only report on simulation results and not experimental results.

Given the lack of analytical predictions and experimental demonstrations regarding jitter's effect on motion control system positioning error, the contributions of this paper are: (1) establishing a simplified discrete model for systems with sampling jitter and control jitter; (2) providing a formula to analytically predict jitter's effect on motion control system positioning error, without requiring simulation; (3) proposing a simple add-on jitter compensator to mitigate jitter's effect on regulation error, without requiring the existing motion controller to be changed; and (4) experimentally demonstrating the effect of sampling jitter and control jitter on positioning error for both regulation and tracking scenarios.

This paper is organized as follows. Section 2 begins by developing a discrete model that captures the interaction between jitter and other signals in a motion control system. Based on this model, analyses are carried out in Section 3 to determine the relationship between jitter and positioning error for two scenarios: (1) regulation error from jitter's interaction with random measurement noise and (2) tracking error from jitter's interaction with a deterministic reference command. Further, with insights obtained from these analyses, several methods to mitigate the positioning degradation due to jitter are discussed, including a new jitter compensator that can be easily added to an existing controller without affecting the controller performance. Lastly, Section 4 presents experimental results for a high-speed precision machine tool for various jitter conditions. These results clearly demonstrate the additional positioning error arising due to jitter and also experimentally validate the model and analyses presented in this paper.

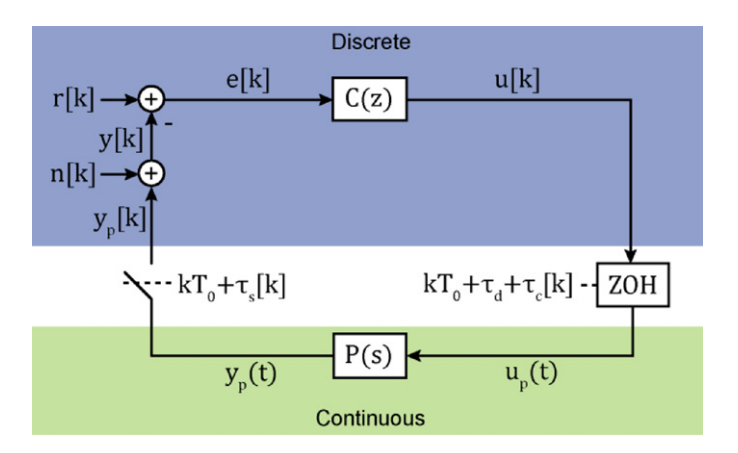


Fig. 1. A digital control feedback system with non-ideal sampler and ZOH.

2. Modeling of digital control systems with non-ideal sampler and ZOH

The block diagram of a typical digitally controlled single-input single-output system is shown in Fig. 1. The plant input signal $u_p(t)$ is related to the plant output signal $y_p(t)$ by

$$\frac{Y_p(s)}{U_p(s)} = P(s),\tag{1}$$

where P(s) is the plant transfer function in the s-domain, and $U_p(s)$ and $Y_p(s)$ are the Laplace-transforms of $u_p(t)$ and $y_p(t)$, respectively. The plant output signal is subsequently sampled by a non-ideal sampler to produce a discrete sequence

$$y_p[k] = y_p(kT_0 + \tau_s[k]),$$
 (2)

where T_0 is the mean value of the digital controller sampling period, k is the integer index of sampling events, and $\tau_s[k]$ is the kth sampling timing deviation from an ideal sampler. In addition to the discrete plant output signal $y_p[k]$, the discrete feedback signal y[k] also includes the noise component n[k], which contains analog-to-digital (ADC) conversion noise, quantization noise, and sampled sensor measurement noise. The control error signal e[k] is then generated by subtracting y[k] from the reference command r[k]. The control sequence signal u[k] is then calculated as

$$\frac{U(z)}{E(z)} = C(z),\tag{3}$$

where C(z) is the controller transfer function in Z-domain, and E(z) and U(z) are the Z-transforms of the discrete signals e[k] and u[k], respectively. The discrete control signal u[k] is finally converted by a non-ideal ZOH to the plant input signal

$$u_p(t) = u[k], \text{ for } kT_0 + \tau_d$$

 $+ \tau_c[k] < t \le (k+1)T_0 + \tau_d + \tau_c[k+1],$ (4)

where τ_d represents the mean latency from the sampler sampling instant to the ZOH update instant, and $\tau_c[k]$ is the update timing deviation from an ideal uniformly spaced ZOH. In this paper, the timing deviations $\tau_s[k]$ and $\tau_c[k]$ are referred as sampling jitter and control jitter, respectively.

Although ideal samplers and ideal ZOHs are used almost exclusively in sampled-data control textbooks [1,2], they do not exist in reality as there is always some sampling jitter, sampling-to-ZOH latency, and control jitter resulting from implementation. The measurement of jitter for several real-time computers used for implementing digital controllers is described in Appendix A. For commercially available control hardware, jitter typically ranges from hundreds of nanoseconds to tens of microseconds.

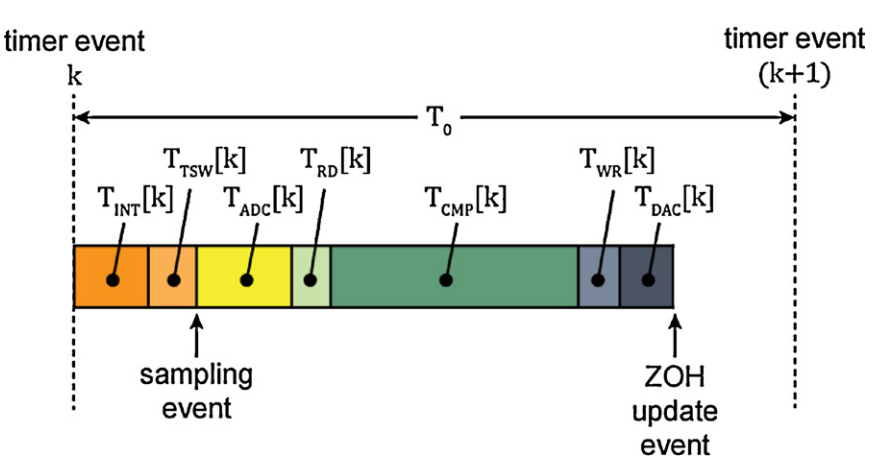


Fig. 2. The sequential timing process of a typical digital control cycle.

In order to illustrate the sources of these non-ideal control timing effects, Fig. 2 shows an example timing process for a digital controller. Each control cycle is initiated by the expiring event of a control cycle timer in the digital control hardware, which is then followed by the interrupt latency $T_{INT}[k]$ and task switching delay $T_{TSW}[k]$ before the sampling of $y_p(t)$ occurs. The control process then needs to wait during the ADC conversion time $T_{ADC}[k]$. After reading the ADC result over a short time $T_{RD}[k]$, the control output is computed in time $T_{CMP}[k]$ using the implemented control algorithm. This computation result is then written to the digital-to-analog converter (DAC) in time $T_{WR}[k]$. Finally, at the end of the DAC conversion time $T_{DAC}[k]$, the analog signal $u_p(t)$ is updated, which corresponds to the ZOH update event.

In such a process, sampling jitter is determined by the timing variation between the timer event and the sampling event,

$$\tau_{\rm S}[k] = \tilde{T}_{\rm INT}[k] + \tilde{T}_{\rm TSW}[k]. \tag{5}$$

Here, the symbol $\tilde{T}[k]$ represents the alternating (AC) component of T[k] (i.e. T[k] subtracted by its mean value \bar{T}). The control cycle timer is usually a hardware device working at several hundred megahertz and can be considered a jitter free event (i.e. the events are perfectly spaced with a constant sampling time T_0). Control jitter $\tau_c[k]$ is then determined by the accumulated timing variation from the timer event to the ZOH update,

$$\tau_{c}[k] = \tilde{T}_{INT}[k] + \tilde{T}_{TSW}[k] + \tilde{T}_{ADC}[k] + \tilde{T}_{RD}[k] + \tilde{T}_{CMP}[k] + \tilde{T}_{WR}[k] + \tilde{T}_{DAC}[k].$$

$$(6)$$

Based on this analysis, both sampling jitter $\tau_s[k]$ and control jitter $\tau_c[k]$ are zero-mean variables. Lastly, the sampling-to-ZOH latency can be expressed as the mean delay from the sampler sampling to the ZOH update,

$$\tau_d = \bar{T}_{ADC} + \bar{T}_{RD} + \bar{T}_{CMP} + \bar{T}_{WR} + \bar{T}_{DAC} \,. \tag{7}$$

This latency can be separated from the non-ideal ZOH in Fig. 1, resulting in a pure delay element and a zero-latency ZOH with jitter as shown in Fig. 3. The expression for the continuous control output u(t) and plant input $u_p(t)$ is then

$$u(t) = u[k]$$
 for $kT_0 + \tau_c[k] < t \le (k+1)T_0 + \tau_c[k+1]$ (8)

$$u_n(t) = u(t - \tau_d). \tag{9}$$

The digital control system model in Fig. 3 is time-variant and thus cannot be analyzed using classical sampled-data control theory. In order to investigate digital control systems with sampling jitter and control jitter, simplified models to approximate the non-ideal sampler and ZOH are developed below.

2.1. Modeling of ZOH with control jitter

In Fig. 4(a), the non-ideal ZOH output signal u(t) is compared with the signal

$$u^*(t) = u[k], \text{ for } kT_0 < t \le (k+1)T_0,$$
 (10)

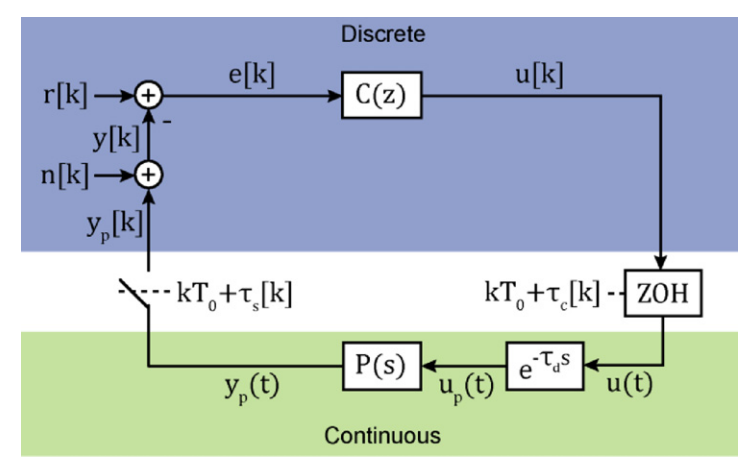
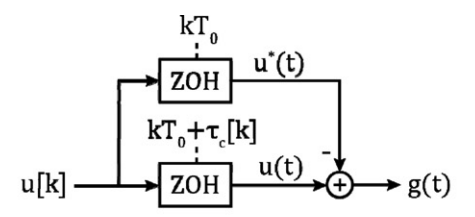
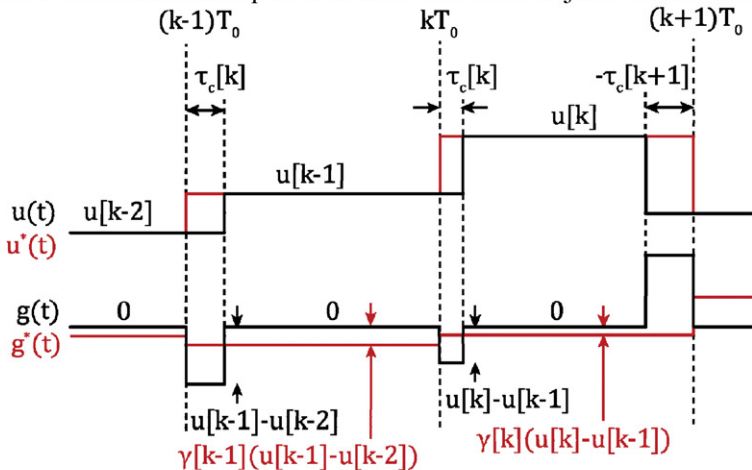


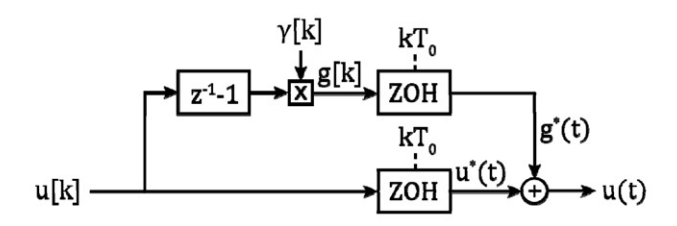
Fig. 3. Equivalent model of a digital control feedback system with non-ideal sampler and ZOH.



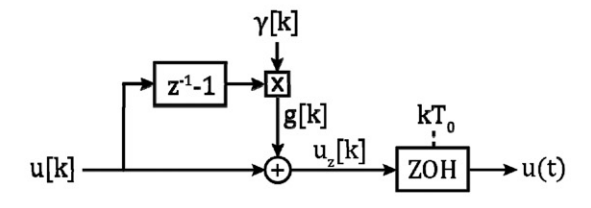
(a) Comparison between the output of a ZOH with control jitter and an ideal ZOH.



(b) Comparison of waveforms between the output of a ZOH with control jitter and an ideal ZOH.



(c) Approximation of jitter disturbance signal g(t).



(d) Approximate model of ZOH with control jitter.

Fig. 4. Modeling of a non-ideal ZOH with control jitter.

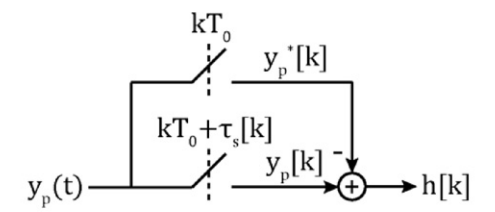
which is the result of control sequence u[k] passing through an ideal ZOH (i.e. the update times are evenly spaced with no variation). The difference between u(t) and $u^*(t)$ due to control jitter is represented by a disturbance signal

$$g(t) = u(t) - u^*(t).$$
 (11)

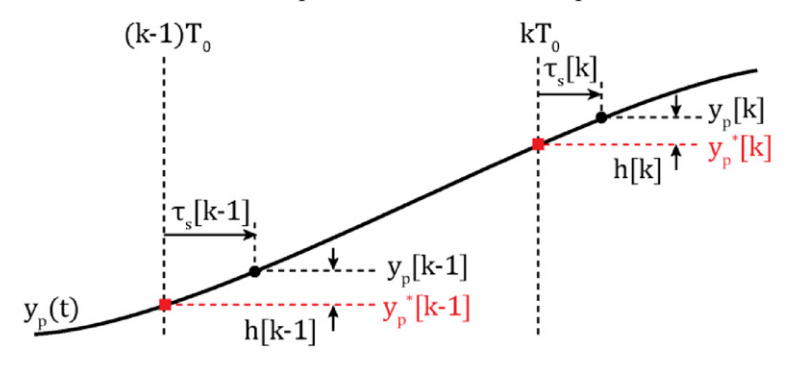
As shown in Fig. 4(b), the g(t) waveform is composed of a pulse train, which is zero everywhere except in the regions when the non-ideal ZOH with jitter leads or lags the ideal ZOH. While

jitter is a discrete phenomenon, this disturbance g(t) is a continuous time signal with sub-sample dynamics. Assuming the sampling rate is much greater than the highest plant dynamics, which is typical for control systems, the disturbance g(t) can be approximated as a piecewise-constant signal

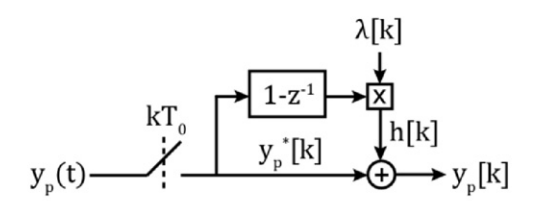
$$g^{*}(t) = (u[k-1] - u[k]) \frac{\tau_{c}[k]}{T_{0}} = (u[k-1] - u[k])\gamma[k],$$
for $kT_{0} < t \le (k+1)T_{0},$ (12)



(a) Comparison between the output sequence of a sampler with sampling jitter and the output sequence of an ideal sampler.



(b) Linear interpolated approximation of disturbance signal h[k]



(c) Approximate model of sampler with sampling jitter.

Fig. 5. Modeling of a non-ideal sampler with sampling jitter.

where $\gamma[k]$ is referred to as the normalized control jitter

$$\gamma[k] = \frac{\tau_c[k]}{T_0}. (13)$$

This selection for $g^*(t)$ conserves the signal momentum (amplitude integration over time) within each sampling period. Further, $g^*(t)$ can now be represented as the output of a discrete signal g[k] passing through an ideal ZOH, as shown in Fig. 4(c), where

$$g(k) = u[k](z^{-1} - 1)\gamma[k]. \tag{14}$$

The two ideal ZOHs from Fig. 4(c) can be combined together as shown in Fig. 4(d). Consequently, the non-ideal ZOH with control jitter in Fig. 3 can be replaced by this disturbance model with an ideal ZOH, thus allowing the analysis to proceed without subsampling dynamics.

2.2. Modeling of sampler with sampling jitter

In Fig. 5(a), the non-ideal sampled plant output signal $y_p[k]$ is compared with the signal

$$y_p^*[k] = y_p(kT), \tag{15}$$

which is the result of $y_p(t)$ going through an ideal sampler (i.e. the sampling times are evenly spaced). The difference between $y_p[k]$

and $y_p^*[k]$ due to sampling jitter is represented by a disturbance signal

$$h[k] = y_p[k] - y_p^*[k]. (16)$$

Fig. 5(b) shows the sampled discrete sequences of $y_p[k]$ and $y_p^*[k]$. As the sampling rate is usually much greater than the plant's highest frequency of interest, the difference h[k] can be approximated by a linear interpolated prediction expressed as

$$h[k] \approx \tau_{s}[k] \left(\frac{y_{p}^{*}[k] - y_{p}^{*}[k-1]}{T_{0}} \right) = \lambda[k](y_{p}^{*}[k] - y_{p}^{*}[k-1]), \quad (17)$$

where

$$\lambda[k] = \frac{\tau_{\rm s}[k]}{T_0}.\tag{18}$$

 $\lambda[k]$ is defined as the normalized sampling jitter. Using this approximation, the discrete sequence $y_p[k]$ sampled by a non-ideal sampler can be modeled by the block diagram in Fig. 5(c), which incorporates the sampling jitter as a disturbance with no sub-sampling dynamics, and uses an ideal sampler. This sampling model is very similar to the control jitter model from Fig. 4(d), with the only difference being where the disturbance enters the control system.

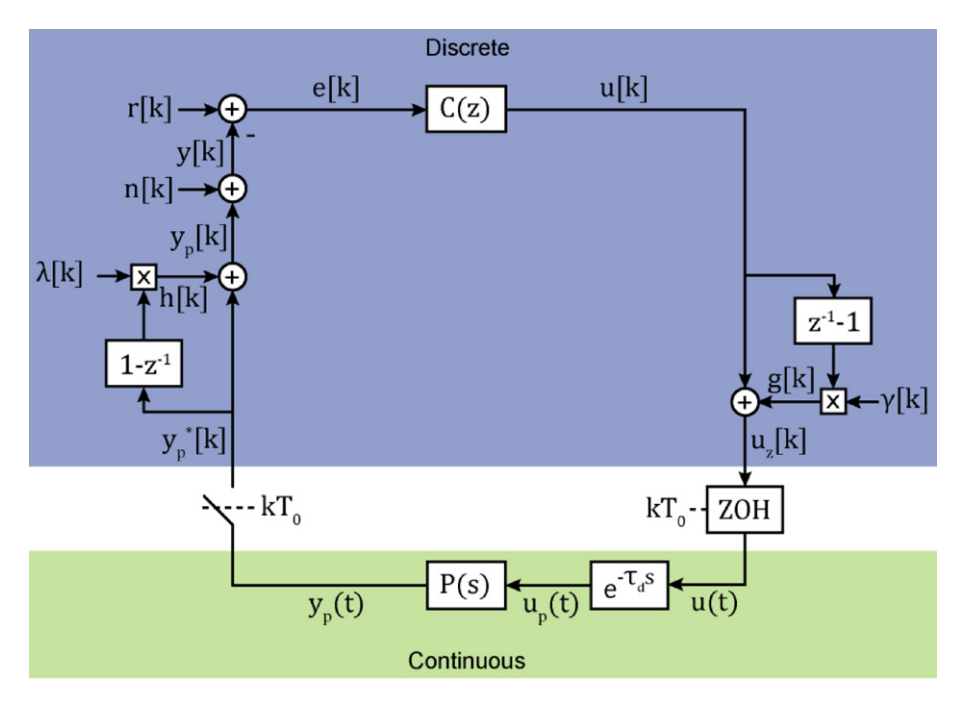


Fig. 6. litter disturbance model of a digital control feedback system with non-ideal sampler and ZOH.

2.3. Simplified model of realistic digital control systems

Replacing the non-ideal sampler and the non-ideal ZOH in Fig. 3 with the models developed in Sections 2.1 and 2.2, results in the overall digital control system model shown in Fig. 6. The effects of jitter are incorporated as two disturbances h[k] and g[k] injected into the system at the ideal sampler and ideal ZOH, respectively. Further, applying ZOH equivalence [1], the dynamic process from $u_z[k]$ through the plant to $y_n^*[k]$ can be represented as

$$P_{z}(z) = \frac{Y_{p}^{*}(z)}{U_{z}(z)} = (1 - z^{-1}) \mathcal{Z} \left\{ \frac{P(s) e^{-\tau_{d} s}}{s} \right\}, \tag{19}$$

where $\mathbb{Z}\{\cdot\}$ is the *Z*-transform of the continuous system impulse response sampled with period T_0 , and $U_z(z)$ and $Y_p^*(z)$ are the *Z*-transforms of $u_z[k]$ and $y_p^*[k]$, respectively. Assuming a proper anti-aliasing filter is implemented, the discrete domain frequency response of P(s) can be calculated as

$$P_{z}(e^{j\omega T_{0}}) = \frac{P(j\omega)e^{-j\omega\tau_{d}}(1 - e^{-j\omega T_{0}})}{j\omega T_{0}}$$
$$= P(j\omega)e^{-j\omega(\tau_{d} + T_{0}/2)}\operatorname{sinc}\left(\frac{\omega T_{0}}{2}\right). \tag{20}$$

As a result, the time-variant digital control system model from Fig. 1 has been converted to the entirely discrete, time-invariant model in Fig. 7. This discrete-time model can enable an intuitive understanding of jitter's effects on control performance. In the next section jitter's effect on positioning error is analyzed using this model.

At this point some insights can be obtained regarding jitter's effects on control performance. First, the magnitude of the jitter disturbances are proportional to the ratio of absolute jitter over the sampling period, and thus high-speed systems that require faster sampling rates will be more susceptible to jitter. Second, the jitter disturbances are a result of derivative interactions with other system signals, such as the reference command and measurement noise, thus the higher frequency content of these other inputs will contribute most to the jitter disturbances. Lastly, the time domain

multiplication that occurs as part of each jitter disturbance can also be viewed in the frequency domain as modulation, thus high frequency interactions between jitter and the other system inputs can result in low frequency disturbances.

3. Analysis of jitter's effect on positioning error

As shown from modeling, the normalized sampling and control jitter $\lambda[k]$ and $\gamma[k]$ disturb the digital control system by modulating the discrete derivatives of the feedback signal and control output signal, respectively. Using the discrete model from Fig. 7, this section analyzes the effects of the jitter disturbances for two scenarios: (1) regulation error resulting from jitter's interaction with measurement noise n[k] and (2) tracking error resulting from jitter's interaction with a reference command r[k]. The positioning error (regulation or tracking) $\varepsilon[k]$ is defined as the desired plant output (reference command) minus the actual plant output sampled by an ideal sampler,

$$\varepsilon[k] = r[k] - y_n^*[k]. \tag{21}$$

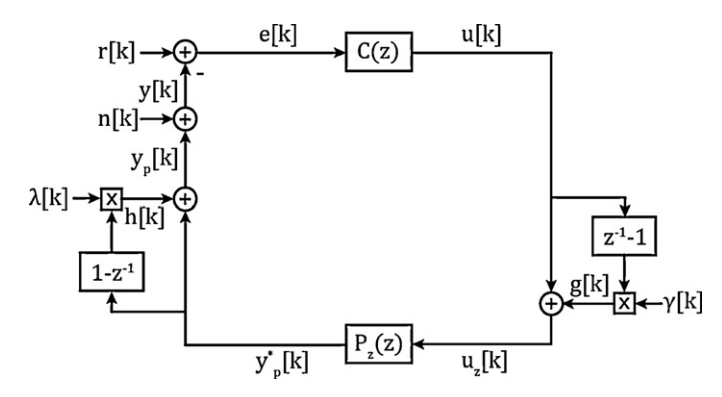


Fig. 7. Fully discrete jitter disturbance model of a digital control system with non-ideal sampler and ZOH.

It should be noted that this definition of positioning error $\varepsilon[k]$ is different from the control error e[k] = r[k] - y[k] (the desired plant output minus the sampled sensor feedback), due to the presence of measurement noise and sampling jitter. Positioning error $\varepsilon[k]$ has been selected for evaluation because it represents the control system performance with more fidelity than the feedback error e[k].

As jitter and measurement noise signals are primarily random, normalized jitters, $\lambda[k]$ and $\gamma[k]$, and measurement noise, n[k], are assumed to be stationary white noise with variances σ_{λ}^{2} , σ_{γ}^{2} , and σ_{n}^{2} , respectively. Accordingly, their auto-correlation functions are.

$$\sigma_h^2 = E(h^2[k]) = \sigma_\lambda^2 \sigma_n^2 \frac{1}{2\pi} \int_{-\pi}^{\pi} \left| \frac{P_z(e^{j\Omega})C(e^{j\Omega})(e^{-j\Omega} - 1)}{1 + P_z(e^{j\Omega})C(e^{j\Omega})} \right|^2 d\Omega, \quad (33)$$

where $E(\cdot)$ is the expected value operation and Ω is frequency in rad/sample. The power spectrum density function (PSD), which is the Fourier transform of a signal's auto-correlation, can be computed for each regulation error components in Eq. (26). Accordingly, the PSD of $\varepsilon_n[k]$, $\varepsilon_g[k]$, and $\varepsilon_h[k]$ are

$$\Phi_{\varepsilon\varepsilon}^{n}(e^{i\omega T_0}) = \sigma_n^2 \left| \frac{P_z(e^{i\omega T_0})C(e^{i\omega T_0})}{1 + P_z(e^{i\omega T_0})C(e^{i\omega T_0})} \right|^2$$
(34)

$$\Phi_{\varepsilon\varepsilon}^{g}(e^{j\omega T_{0}}) = \sigma_{n}^{2}\sigma_{\gamma}^{2} \left(\frac{1}{2\pi} \int_{-\pi}^{\pi} \left| \frac{C(e^{j\Omega})(1 - e^{-j\Omega})}{1 + P_{z}(e^{j\Omega})C(e^{j\Omega})} \right|^{2} d\Omega \right) \left| \frac{P_{z}(e^{j\omega T_{0}})}{1 + P_{z}(e^{j\omega T_{0}})C(e^{j\omega T_{0}})} \right|^{2}$$

$$(35)$$

$$\Phi_{\varepsilon\varepsilon}^{h}(e^{j\omega T_{0}}) = \sigma_{n}^{2}\sigma_{\lambda}^{2} \left(\frac{1}{2\pi} \int_{-\pi}^{\pi} \left| \frac{P_{z}(e^{j\Omega})C(e^{j\Omega})(e^{-j\Omega} - 1)}{1 + P_{z}(e^{j\Omega})C(e^{j\Omega})} \right|^{2} d\Omega \right) \left| \frac{P_{z}(e^{j\omega T_{0}})C(e^{j\omega T_{0}})}{1 + P_{z}(e^{j\omega T_{0}})C(e^{j\omega T_{0}})} \right|^{2}.$$

$$(36)$$

$$\phi_{nn}[k] = \sigma_n^2 \delta[k] \tag{22}$$

$$\phi_{\lambda\lambda}[k] = \sigma_{\lambda}^2 \delta[k] \tag{23}$$

$$\phi_{\gamma\gamma}[k] = \sigma_{\gamma}^2 \delta[k]. \tag{24}$$

where $\delta[k]$ is the Dirac delta function, $\phi_{xx}[k]$ is the autocorrelation of signal x[k], as used for stochastic signal analysis in [26].

3.1. Regulation error analysis

For position regulation, the reference command can be assumed to be zero without loss of generality: $r[k] = 0 \quad \forall \quad k$. Consequently, the positioning error in the regulation case (regulation error) reduces to

$$\varepsilon[k] = -y_n^*[k]. \tag{25}$$

By decomposing the regulation error into components of measurement noise n[k], control jitter disturbance g[k], and sampling jitter disturbance h[k], it can be expressed as

$$\varepsilon[k] = \varepsilon_n[k] + \varepsilon_g[k] + \varepsilon_h[k], \tag{26}$$

where

$$\varepsilon_n[k] = n[k] * Z^{-1} \left(\frac{P_Z(z)C(z)}{1 + P_Z(z)C(z)} \right)$$
 (27)

$$\varepsilon_g[k] = g[k] * \mathbf{Z}^{-1} \left(\frac{-P_z(z)}{1 + P_z(z)C(z)} \right)$$
 (28)

$$\varepsilon_h[k] = h[k] * Z^{-1} \left(\frac{P_Z(z)C(z)}{1 + P_Z(z)C(z)} \right).$$
 (29)

Here, * is the convolution operation, and $\mathbf{Z}^{-1}(\cdot)$ is the inverse Z-transform operation. Considering that $\gamma[k]$ and $\lambda[k]$ are typically only a few percent, second-order and higher interactions are negligible. This simplifies the expressions for the jitter disturbances to

$$g[k] = \gamma[k] \left[n[k] * Z^{-1} \left(\frac{C(z) \left(1 - z^{-1} \right)}{1 + P_z(z)C(z)} \right) \right]$$
 (30)

$$h[k] = \lambda[k] \left[n[k] * Z^{-1} \left(\frac{P_z(z)C(z) \left(z^{-1} - 1 \right)}{1 + P_z(z)C(z)} \right) \right].$$
 (31)

Therefore, g[k] and h[k] are white noises with variances equal to

$$\sigma_g^2 = E(g^2[k]) = \sigma_\gamma^2 \sigma_n^2 \frac{1}{2\pi} \int_{-\pi}^{\pi} \left| \frac{C(e^{j\Omega}) \left(1 - e^{-j\Omega} \right)}{1 + P_z(e^{j\Omega}) C(e^{j\Omega})} \right|^2 d\Omega$$
 (32)

 $\varepsilon_n[k]$ and $\varepsilon_h[k]$'s PSDs can thus be compared as

$$\frac{\Phi_{\varepsilon\varepsilon}^{h}(e^{j\omega T_{0}})}{\Phi_{\varepsilon\varepsilon}^{n}(e^{j\omega T_{0}})} = \sigma_{\lambda}^{2} \left(\frac{1}{2\pi} \int_{-\pi}^{\pi} \left| \frac{P_{z}(e^{j\Omega})C(e^{j\Omega})(e^{-j\Omega} - 1)}{1 + P_{z}(e^{j\Omega})C(e^{j\Omega})} \right|^{2} d\Omega \right). \quad (37)$$

For a properly designed control system, $\left|(P_Z(e^{j\Omega})C(e^{j\Omega})(e^{-j\Omega}-1))/(1+P_Z(e^{j\Omega})C(e^{j\Omega}))\right|$ is much less than 2 for all frequencies. As a result,

$$\frac{1}{2\pi} \int_{-\pi}^{\pi} \left| \frac{P_z(e^{j\Omega})C(e^{j\Omega})(e^{-j\Omega} - 1)}{1 + P_z(e^{j\Omega})C(e^{j\Omega})} \right|^2 d\Omega < 4. \tag{38}$$

Considering that the normalized sampling jitter standard deviation σ_{λ} in most digital control systems is less than 0.1, $\varepsilon_{n}[k]$ and $\varepsilon_{h}[k]$'s PSDs ratio is approximately

$$\frac{\Phi_{\varepsilon\varepsilon}^{h}(e^{j\omega T_0})}{\Phi_{\varepsilon\varepsilon}^{n}(e^{j\omega T_0})} < 4\sigma_{\lambda}^2 < 0.04. \tag{39}$$

Therefore, sampling jitter has a negligible effect on regulation error, and the total regulation error reduces to $\varepsilon[k] = \varepsilon_n[k] + \varepsilon_g[k]$. As control jitter $\gamma[k]$ and measurement noise n[k] are generally uncorrelated, the PSD of the regulation error can be expressed as

$$\Phi_{\varepsilon\varepsilon}(e^{j\omega T_0}) = \Phi_{\varepsilon\varepsilon}^n(e^{j\omega T_0}) + \Phi_{\varepsilon\varepsilon}^g(e^{j\omega T_0}). \tag{40}$$

From expression of $\Phi^{\mathbf{g}}_{\varepsilon\varepsilon}(e^{j\omega T_0})$ in Eq. (35), it can be seen that control jitter operates primarily on the high frequency controller gain to produce a low frequency disturbance, which is counteracted by the controller's disturbance rejection response. Consequently, the presence of control jitter will contribute additional regulation error to the digital control system. Integrating the PSD, the root-mean-square (RMS) regulation error can be calculated as

$$\sigma_{\varepsilon}^{2} = \sigma_{n}^{2} \left(\frac{1}{2\pi} \int_{-\pi}^{\pi} \left| \frac{P_{z}(e^{j\Omega})C(e^{j\Omega})}{1 + P_{z}(e^{j\Omega})C(e^{j\Omega})} \right|^{2} d\Omega \right)$$

$$+ \sigma_{n}^{2} \sigma_{\gamma}^{2} \left(\frac{1}{2\pi} \int_{-\pi}^{\pi} \left| \frac{C(e^{j\Omega}) \left(1 - e^{-j\Omega} \right)}{1 + P_{z}(e^{j\Omega})C(e^{j\Omega})} \right|^{2} d\Omega \right)$$

$$\times \left(\frac{1}{2\pi} \int_{-\pi}^{\pi} \left| \frac{P_{z}(e^{j\Omega})}{1 + P_{z}(e^{j\Omega})C(e^{j\Omega})} \right|^{2} d\Omega \right)$$

$$(41)$$

In this result, the first term is the regulation error contribution from measurement noise and the second term is the contribution from control jitter. The overall regulation error magnitude is dependent on the measurement noise, normalized control jitter, controller gain, and controller disturbance rejection.

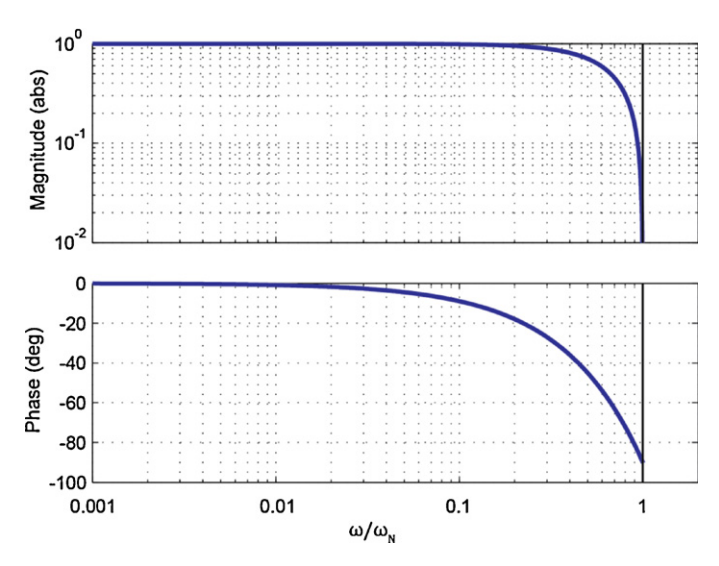


Fig. 8. Frequency response of the jitter compensator for mitigating control jitter disturbance on regulation error. ω_N is the system's Nyquist frequency.

3.1.1. Solutions to jitter effect on regulation error

There are several methods that can be used to mitigate control jitter's effect on the regulation error. Since the jitter disturbance enters the closed-loop as a disturbance at the plant input, one method is to increase the controller disturbance rejection capability. This attenuates the term $\frac{1}{2\pi}\int_{-\pi}^{\pi}\left|P_{z}(e^{j\Omega})/(1+P_{z}(e^{j\Omega})C(e^{j\Omega}))\right|^{2}d\Omega$ from Eq. (41); however, stability constraints will impose limits on the attainable disturbance rejection of the controller. A second method is to reduce the litter magnitude by improving task handling in operation system or switching to better controller hardware with less jitter. A third method is to attenuate the controller gain near the system Nyquist frequency $\omega_N = \pi/T_0$. This greatly attenuates the term $\frac{1}{2\pi} \int_{-\pi}^{\pi} \left| (C(e^{j\Omega})(1 - e^{-j\Omega}))/(1 + P_z(e^{j\Omega})C(e^{j\Omega})) \right|^2 d\Omega$ in Eq. (41), as its magnitude is primarily determined by high frequency signal content due to the high-pass filtering effect of $1 - e^{-j\Omega}$. This can be done by cascading a jitter compensator $C_g(z)$, which consists of a zero at the Nyquist frequency, with the existing controller. The expression for this jitter compensator is

$$C_g(z) = \frac{1 + z^{-1}}{2}. (42)$$

Fig. 8 shows the frequency response of $C_g(z)$ as a function of normalized frequency. $C_g(z)$ has little effect on controller gain and phase for frequencies less than one-tenth of the Nyquist frequency, but greatly attenuates controller gain near the Nyquist frequency. As a result, this jitter compensator can be directly cascaded with an existing controller, largely mitigating the effect of control jitter on regulation without requiring redesign of the existing controller.

3.2. Tracking error analysis

In the tracking case the measurement noise is assumed to be zero (n[k] = 0) and the reference command r[k] is a deterministic signal. By decomposing the positioning error (tracking error) into components from reference signal r[k], control jitter disturbance g[k], and sampling jitter disturbance h[k], it can be expressed as

$$\varepsilon[k] = r[k] - y_n^*[k] = \varepsilon_r[k] + \varepsilon_g[k] + \varepsilon_h[k], \tag{43}$$

where

$$\varepsilon_r[k] = r[k] * Z^{-1} \left(\frac{1}{1 + P_r(z)C(z)} \right)$$

$$\tag{44}$$

$$\varepsilon_g[k] = g[k] * Z^{-1} \left(\frac{-P_z(z)}{1 + P_z(z)C(z)} \right)$$
 (45)

$$\varepsilon_h[k] = h[k] * Z^{-1} \left(\frac{P_z(z)C(z)}{1 + P_z(z)C(z)} \right). \tag{46}$$

 $\varepsilon_r[k]$ is the tracking error when there is no jitter, $\varepsilon_g[k]$ is the tracking error contributed by the control jitter disturbance, and $\varepsilon_h[k]$ is the tracking error contributed by the sampling jitter disturbance. In motion control applications, repetitive command signals are widely used and can be viewed as the sum of M distinctive single-tone signals,

$$r[k] = \sum_{m=1}^{M} R_m \sin(\omega_m k T_0 + \varphi_m), \tag{47}$$

where R_m , ω_m , and φ_m are the mth signal component's amplitude, frequency in rad/s, and phase in rad, respectively. The tracking error for non-repetitive finite-energy deterministic command tracking is analyzed in Appendix B.

In accordance with the discrete model in Fig. 7, the control jitter disturbance signal g[k] can be represented as

$$g[k] = \gamma[k]u_{\Lambda}[k],\tag{48}$$

where $u_{\Delta}[k] = u[k-1] - u[k]$. By ignoring second-order and higher interactions, $u_{\Delta}[k]$ can be expressed as

$$u_{\Delta}[k] = r[k] * Z^{-1} \left(\frac{C(z)(z^{-1} - 1)}{1 + P_z(z)C(z)} \right). \tag{49}$$

The auto-correlation function of g[k] is then

$$\phi_{gg}[k, m] = E(g[k]g[m]) = u_{\Lambda}^{2}[k]\sigma_{\nu}^{2}\delta[m - k]. \tag{50}$$

Therefore, g[k] is a non-stationary white noise signal and its resulting tracking error contribution $\varepsilon_g[k]$ is a non-stationary stochastic signal. Although $\varepsilon_g[k]$'s variance is time-varying, its mean value can be used to evaluate the effect of the control jitter disturbance on positioning error. This is calculated as

$$\overline{E(\varepsilon_{g}^{2}[k])} = \overline{E(g^{2}[k])} \frac{1}{2\pi} \int_{-\pi}^{\pi} \left| \frac{P_{z}(e^{j\Omega})}{1 + P_{z}(e^{j\Omega})C(e^{j\Omega})} \right|^{2} d\Omega$$

$$= \sigma_{\gamma}^{2} \overline{u_{\Delta}^{2}[k]} \frac{1}{2\pi} \int_{-\pi}^{\pi} \left| \frac{P_{z}(e^{j\Omega})}{1 + P_{z}(e^{j\Omega})C(e^{j\Omega})} \right|^{2} d\Omega$$

$$= \sigma_{\gamma}^{2} \left(\sum_{m=1}^{M} \frac{R_{m}^{2}}{2} \left| \frac{C(e^{j\omega_{m}T_{0}})[e^{-j\omega_{m}T_{0}} - 1]}{1 + P_{z}(e^{j\omega_{m}T_{0}})C(e^{j\omega_{m}T_{0}})} \right|^{2} \right)$$

$$\times \left(\frac{1}{2\pi} \int_{-\pi}^{\pi} \left| \frac{P_{z}(e^{j\Omega})}{1 + P_{z}(e^{j\Omega})C(e^{j\Omega})} \right|^{2} d\Omega \right), \tag{51}$$

where $\overline{(\cdot)}$ represents the temporal averaging operation.

Similarly, the sampling jitter disturbance h[k] can be expressed as

$$h[k] = \lambda[k] y_{\Lambda}[k], \tag{52}$$

where $y_{\Delta}[k]=y_p^*[k]-y_p^*[k-1]$. Ignoring second-order and higher terms this can be expressed as

$$y_{\Delta}[k] = r[k] * \mathbf{Z}^{-1} \left(\frac{P_z(z)C(z)(1 - z^{-1})}{1 + P_z(z)C(z)} \right).$$
 (53)

The auto-correlation function of h[k] is then

$$\phi_{hh}[k,m] = E(h[k]h[m]) = y_{\Lambda}^{2}[k]\sigma_{\lambda}^{2}\delta[m-k]. \tag{54}$$

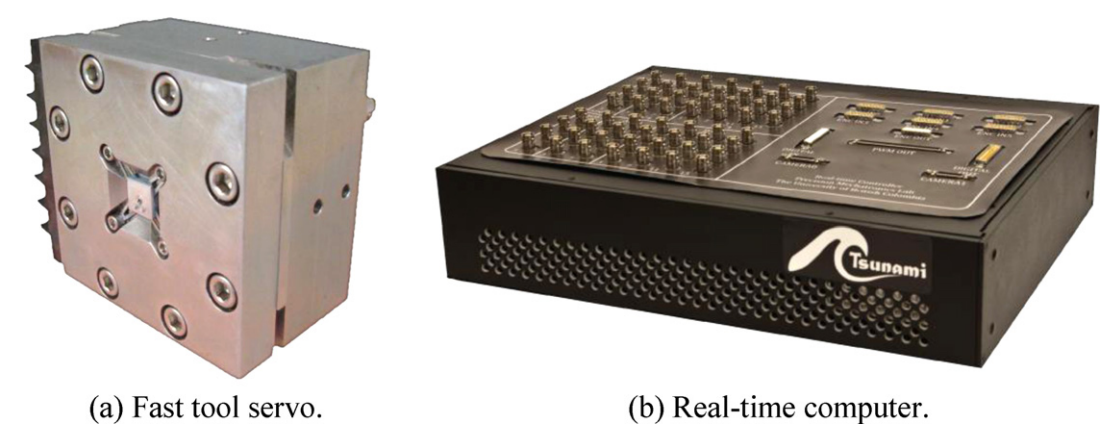


Fig. 9. Experimental setup consisting of a fast-tool servo and custom real-time computer.

Again, h[k] is a non-stationary white noise signal and its resulting tracking error contribution $\varepsilon_h[k]$ is a non-stationary stochastic signal. Thus the mean value of its variance is used to evaluate the effect of the sampling jitter on positioning error, which can be calculated as

$$\overline{E(\varepsilon_{h}^{2}[k])} = \sigma_{\lambda}^{2} \overline{y_{\Delta}^{2}[k]} \frac{1}{2\pi} \int_{-\pi}^{\pi} \left| \frac{P_{z}(e^{j\Omega})C(e^{j\Omega})}{1 + P_{z}(e^{j\Omega})C(e^{j\Omega})} \right|^{2} d\Omega$$

$$= \sigma_{\lambda}^{2} \left(\sum_{m=1}^{M} \frac{R_{m}^{2}}{2} \left| \frac{P_{z}(e^{j\omega_{m}T_{0}})C(e^{j\omega_{m}T_{0}})[1 - e^{-j\omega_{m}T_{0}}]}{1 + P_{z}(e^{j\omega_{m}T_{0}})C(e^{j\omega_{m}T_{0}})} \right|^{2} \right)$$

$$\times \left(\frac{1}{2\pi} \int_{-\pi}^{\pi} \left| \frac{P_{z}(e^{j\Omega})C(e^{j\Omega})}{1 + P_{z}(e^{j\Omega})C(e^{j\Omega})} \right|^{2} d\Omega \right). \tag{55}$$

Lastly, as $\varepsilon_r[k]$ is a deterministic signal, its mean variance is simply its mean-square value,

$$\overline{\varepsilon_r^2[k]} = \sum_{m=1}^M \frac{R_m^2}{2} \left| \frac{1}{1 + P_z(e^{j\omega_m T_0})C(e^{j\omega_m T_0})} \right|^2.$$
 (56)

Generally, $\varepsilon_r[k]$ can be completely eliminated by designing infinite controller gain at frequency ω_m , therefore the remaining tracking error is a result of jitter's interaction with the reference command. The overall tracking error magnitude is then dependent on the reference command, control jitter, sampling jitter, controller gain, and controller disturbance rejection.

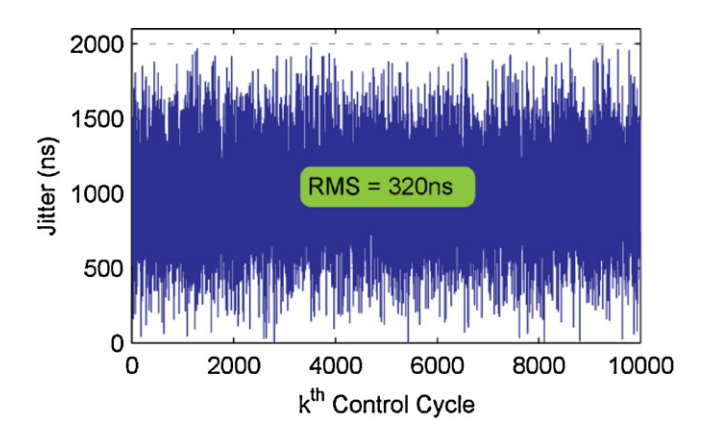
In order to mitigate jitter-contributed tracking error $\varepsilon_g[k]$ and $\varepsilon_h[k]$, the most effective way is to reduce the jitter magnitude, either by software or operating system improvement or by switching to better controller hardware with less jitter. It should be noted that the previously discussed jitter compensator $C_g(z)$ in Eq. (42) is generally not helpful in reducing jitter's effect on tracking error because the frequencies of the reference command are usually far less than the system Nyquist frequency.

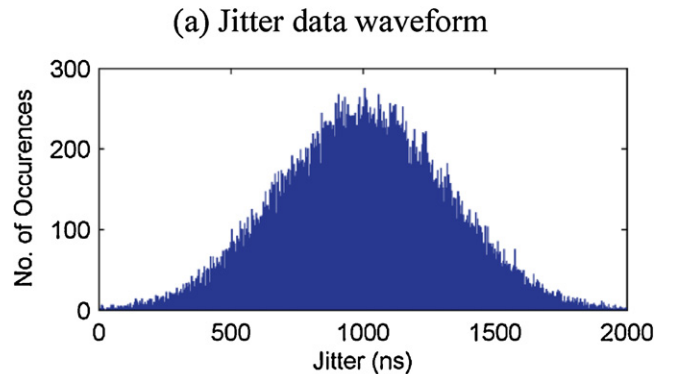
Using Eqs. (41), (51) and (55), jitter's effect on positioning error can be predicted without simulation. A key property of these relations is that they do not require analytical models of the system (such as state space and transfer functions) and an experimentally measured plant frequency response is sufficient to calculate the effect of jitter.

4. Experimental results

Experiments are performed to validate the model and analysis of the jitter disturbance effect presented in this paper. They are conducted on an improved version of the fast-tool servo (FTS)

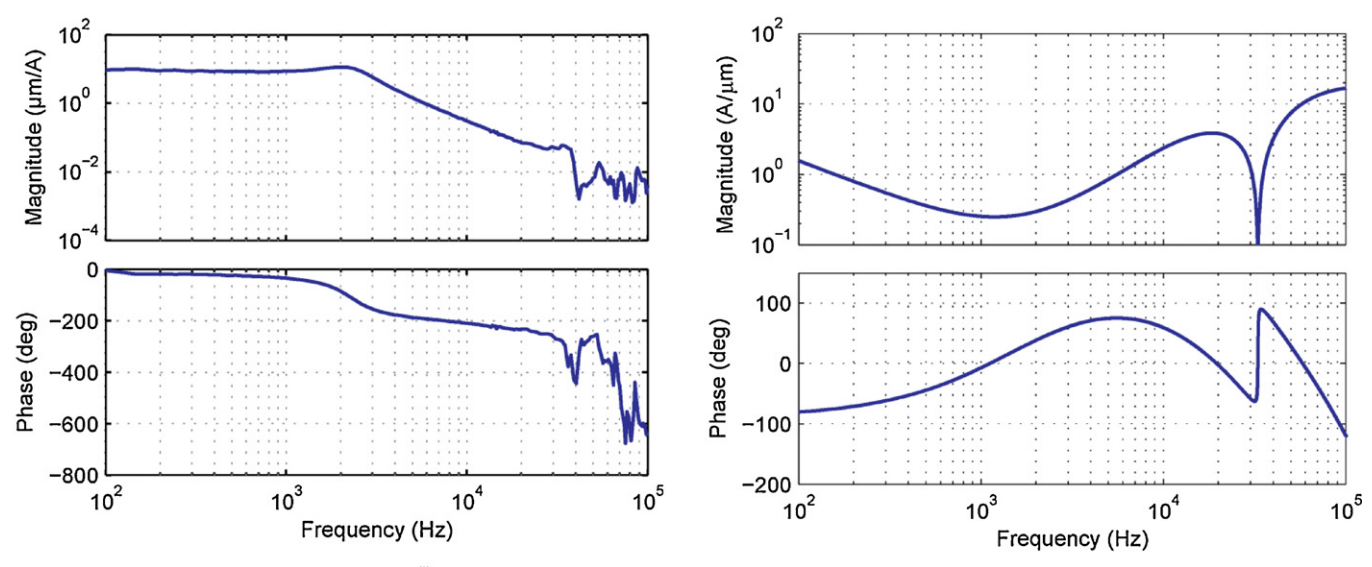
presented in [27], which is a high-bandwidth electro-magnetically actuated precision machine tool that uses a capacitive probe for position feedback. This FTS, shown in Fig. 9(a), can achieve 50 µm stroke, 1.4 nm positioning error, and 750 g acceleration in continuous operation. The digital control hardware is a custom real-time computer made of high-performance digital signal processors and a field programmable gate array [28]. This computer, shown in Fig. 9(b), can achieve a sampling period of 1 µs for floating-point calculation of digital controllers with jitter less than 6 ns RMS. This performance is significantly better than commercial controller hardware, which typically is limited to <100 kHz sampling rate and >100 ns jitter. It should be noted that experimental measurement of jitters' effect on positioning error is very difficult on most commercial control hardware, because they do not provide the option



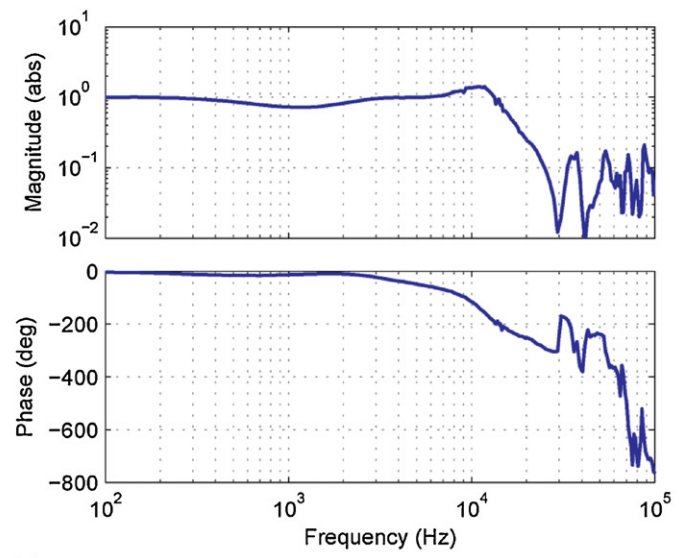


(b) Jitterdata histogram

Fig. 10. 8% RMS normalized jitter data used for the experiments.



- (a) Plant frequency response $P_z(e^{j\omega T_0})$ from current command (A) to position output (μ m).
- (b) Base controller frequency response $C_B(e^{j\omega T_0})$.



(c) Closed-loop frequency response from r[k] to y[k], when the fast tool servo is controlled by the *base controller* $C_B(z)$.

Fig. 11. Frequency responses of the fast-tool servo feedback control system.

to add extra amount of jitters in input and output timing and are unable to achieve very low jitter (such as a few nano-seconds) to establish a benchmark performance without jitter. The real-time controller in Fig. 9(b) is a key enabling tool to investigate jitters' effect experimentally.

Two experimental cases are conducted to demonstrate the effect of jitter on motion control performance: (1) regulation error resulting from jitter's interaction with measurement noise and (2) tracking error resulting from jitter's interaction with reference command. For each case, the sampling jitter and control jitter effects are tested separately.

4.1. Experiment setup

Since the custom control hardware has nearly zero jitter, variable delays is inserted into the real-time controller execution to achieve a deterministic amount of sampling jitter or control jitter. The added jitter uses pre-generated arrays of delay values to produce random white jitter with RMS magnitude ranging from 0 to 400 ns. Fig. 10 shows the added jitter data and histogram for the case of 320 ns RMS. For experiments at other jitter magnitudes, the jitter data in Fig. 10 is scaled accordingly. Although execution of the control algorithm takes less than 1 μ s on the custom control hardware, a sampling period of $T_0=4\,\mu$ s is used throughout all experiments to accommodate additional jitter. Note that the jitter percentage referred to throughout this section is relative to the sampling period, as it refers to the normalized jitter from Eqs. (13) and (18). For example, 160 ns RMS jitter for a 4 μ s sampling period is 4% jitter.

The experimentally measured frequency response of the FTS is shown in Fig. 11(a), from u[k] (input current in Amperes) to y[k] (plant output in μ m). Accordingly, a loop-shaping based controller

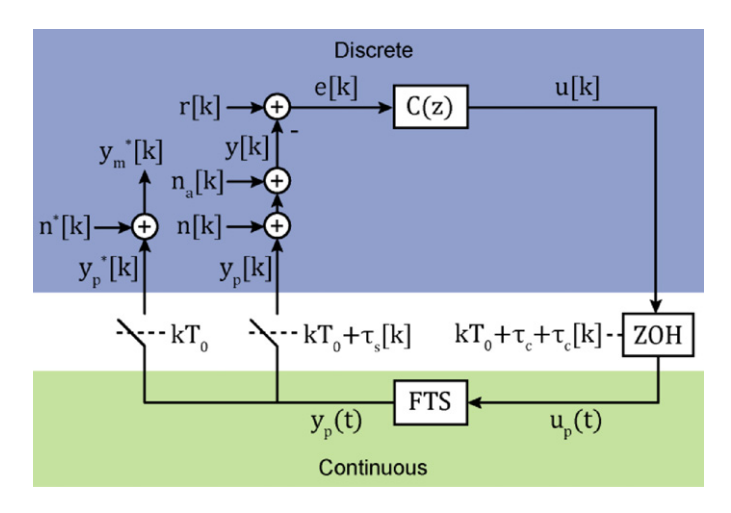


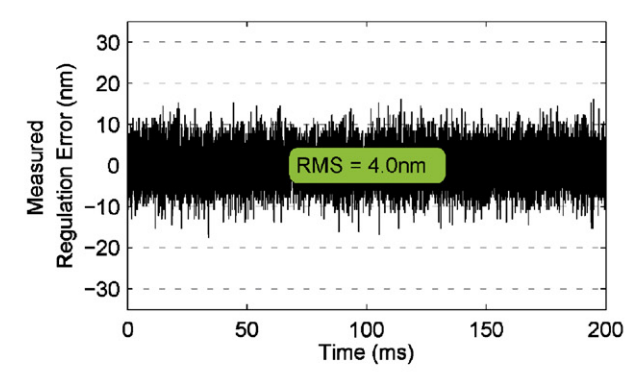
Fig. 12. System block diagram of the experimental setup.

 $C_B(z)$ is designed to control the FTS, as follows:

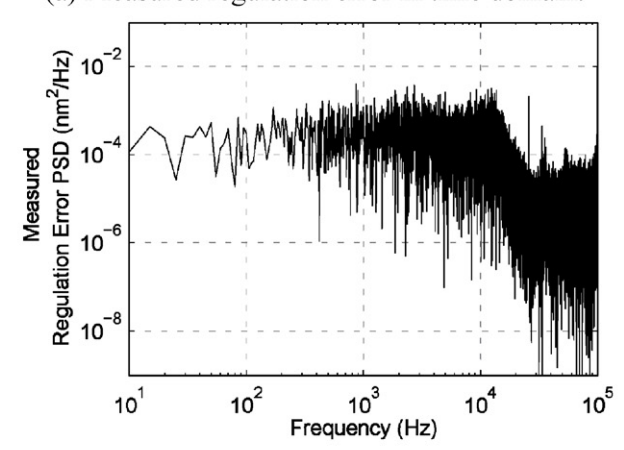
$$C_B(z) = 6.5702 \times \frac{(z - 0.9698)}{(z - 1)} \times \frac{(z - 0.9606)(z - 0.9352)}{(z - 0.3659)(z - 0.5471)(z - 0.081)} \times \frac{(z^2 - 1.3449z - 0.9917)}{(z^2 - 0.8726z - 0.1904)}.$$
(57)

This controller has three components: (1) an integrator that acts from 0 to 1.2 kHz; (2) a double-lead compensator to add phase from 1 kHz to 20 kHz; and (3) a notch filter at 33 kHz to attenuate the plant resonance at this frequency. The controller frequency response is shown in Fig. 10(b). The resulting closed-loop frequency response is shown in Fig. 10(c) and has a -3 dB bandwidth of 15 kHz. Unless otherwise specified, the implemented controller in all the experiments is the loop-shaping base controller, that is $C(z) = C_R(z)$.

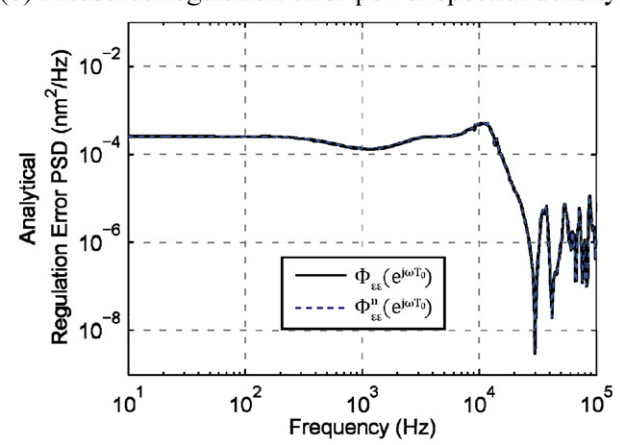
Referring to Fig. 7, it is the positioning error $\varepsilon[k] = r[k] - y_n^*[k]$ and not the control error e[k] = r[k] - y[k] that represents the control system performance. One challenge faced when attempting to experimentally measure jitter's effect is that $y_n^*[k]$ is not readily available due to the presence of measurement noise n[k]and sampling jitter disturbance h[k]. To overcome h[k], a double sampling scheme is implemented in the custom real-time computer, as shown in Fig. 12. In each control cycle, there are two ADC sampling events of the plant output $y_p(t)$: one ADC with sampling jitter is used to acquire y[k] for the controller calculation; another ADC with zero sampled jitter is used to acquire $y_m^*[k]$ for positioning performance evaluation. However, $y_m^*[k]$ still contains measurement noise $n^*[k]$ (the combination of ADC noise and sensor noise, 1.4 nm RMS). In the regulation experiment an additional white noise $n_a[k]$ of 8 nm RMS is added, as shown in Fig. 12, in order to make $n^*[k]$'s contribution negligible, and therefore $y_m^*[k]$ can be used to approximate $y_n^*[k]$. In the tracking experiment the reference signal r[k] amplitude is set at $2 \mu m$, which results in large enough tracking error to dominate the contribution from $n^*[k]$, therefore $y_m^*[k]$ can again be used to approximate $y_n^*[k]$. Still, in both cases there will be a slight difference between the experimentally recorded positioning error and the true plant regulation error due to $n^*[k]$. It follows that the approximated expression for the positioning error used for evaluating the effect of jitter in all the experiments is $\varepsilon[k] \approx r[k] - y_m^*[k]$.



(a) Measured regulation error in time domain.



(b) Measured regulation error power spectral density.

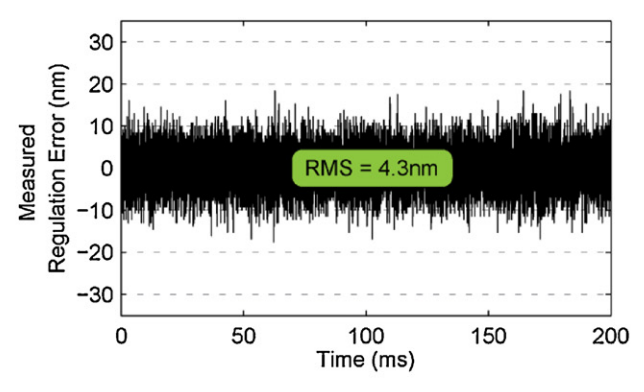


(c) Predicted regulation error power spectral density

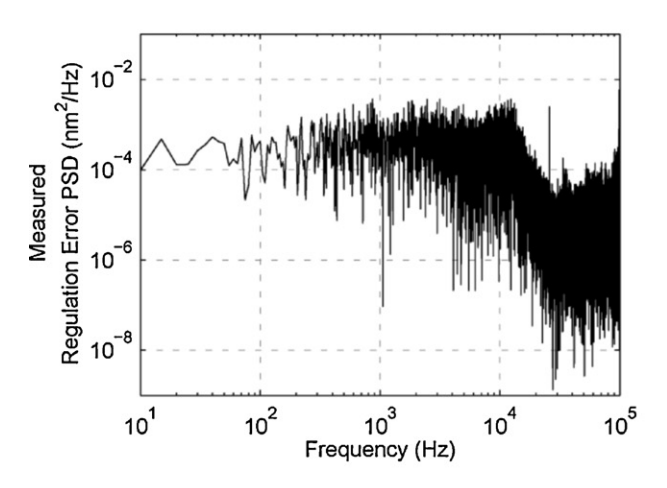
Fig. 13. Regulation error experimental results for no jitter.

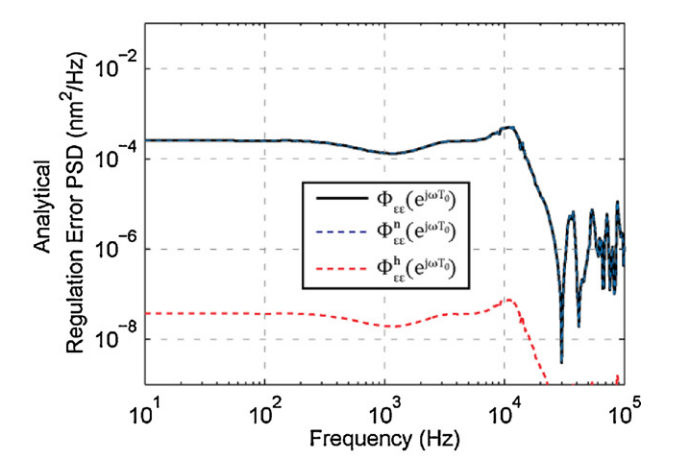
4.2. Regulation error experimental results with white measurement noise

For the regulation error experiment, the reference command r[k] is set at zero and the added measurement noise $n_a[k]$ is a white stochastic 8 nm RMS signal. As a reference benchmark, Fig. 13 shows the measured regulation error for zero sampling jitter and zero control jitter. The measured 4.0 nm RMS regulation error is smaller than the added noise $n_a[k]$ (8 nm RMS) because much of the high frequency noise content is filtered by the plant dynamics. As shown in Fig. 13(b), the regulation error PSD is shaped similarly to the system's closed-loop frequency response



(a) Measured regulation error in time domain.





- (b) Measured regulation error power spectral density.
- (c) Predicted regulation error power spectral density.

Fig. 14. Regulation error experimental results for 8% sampling jitter.

of Fig. 11(c), as predicted by the analytical PSD in Fig. 13(c). The analytical PSD response in Fig. 13(c) is calculated using Eq. (34).

4.2.1. Effect of sampling jitter on regulation error

In this experiment the control jitter is set to zero and the sampling jitter is varied from 0% to 10% of the sampling period using the jitter data from Fig. 10. Fig. 14(a) shows the measured regulation error for 8% sampling jitter. There is no noticeable increase in both the measured error waveform and PSD compared to the 0% jitter reference case from Fig. 13(b). This is consistent with the analytically predicted PSD in Fig. 14(c), calculated from Eqs. (34) and (36). As discussed in Section 3, the sampling jitter contribution to regulation error $\varepsilon_h[k]$ is much less than the measurement noise contribution to regulation error $\varepsilon_n[k]$. For other magnitudes of sampling jitter, the measured and analytical RMS regulation error is plotted in Fig. 15, again confirming the earlier conclusion that the sampling jitter has a negligible effect on regulation error.

4.2.2. Effect of control jitter on regulation error

In this experiment the sampling jitter is set at zero and the control jitter is varied from 0% to 10% of the sampling period using the jitter data from Fig. 10. Fig. 16(a) shows the experimental measured regulation error for 8% control jitter. In comparison with the zero control jitter benchmark result in Fig. 13(a), the 8% control jitter causes the RMS regulation

error to increase by 90%, from 4.0 nm to 7.7 nm. Comparing their PSDs, the major difference in the frequency domain occurs around 1 kHz, which corresponds to the controller's minimum disturbance rejection region. This result is consistent with the

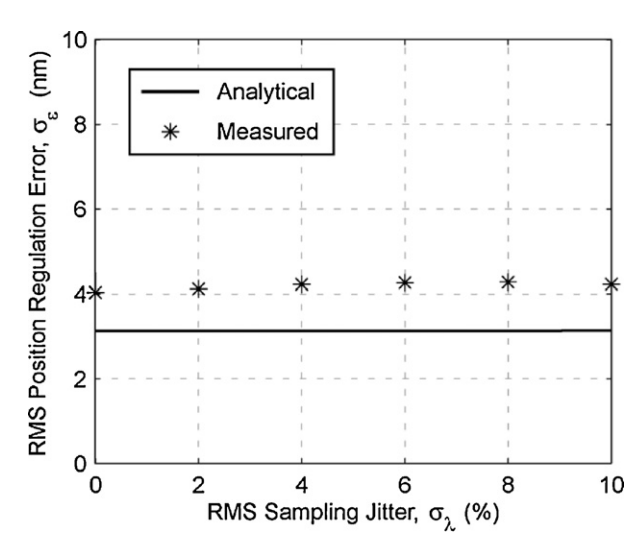
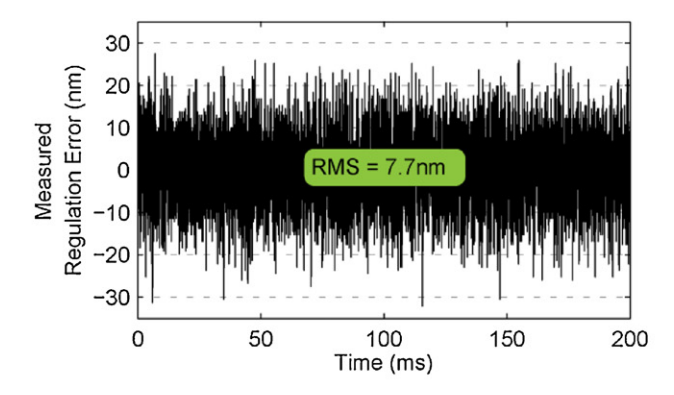
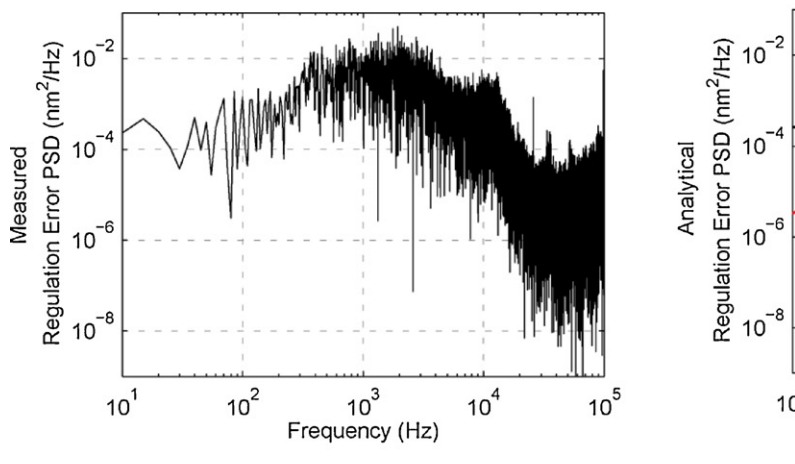
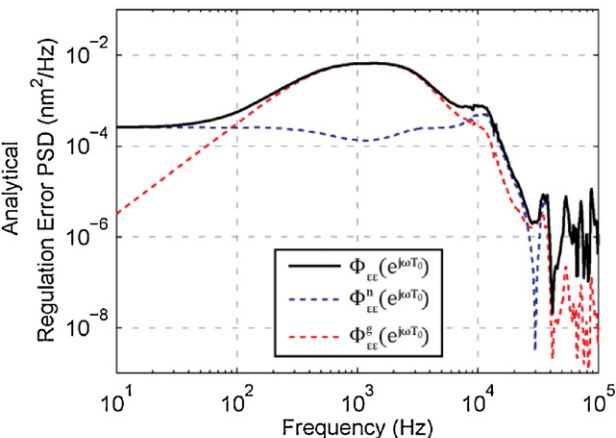


Fig. 15. Measured and analytical RMS regulation error comparison for various amounts of sampling jitter.



(a) Measured regulation error in time domain.





- (b) Measured regulation error power spectral density.
- (c) Predicted regulation error power spectral density.

Fig. 16. Regulation error experimental results for 8% control jitter without jitter compensator.

analytically predicted PSD in Fig. 16(c), which is calculated from Eqs. (35) and (36). The analytical PSD shows that the control jitter contribution to regulation error $\varepsilon_g[k]$ is dominant over the measurement noise contribution to regulation error $\varepsilon_n[k]$ in the frequency range from 100 Hz to 10 kHz, thus causing the total regulation error to increase. This result clearly indicates that control jitter's interaction with measurement noise produces a low frequency disturbance that degrades position regulation performance.

When the proposed jitter compensator $C_g(z)$ is added to the base controller, $C(z) = C_B(z)C_g(z)$, the RMS regulation error greatly decreases from 7.7 nm to 4.7 nm, despite the 8% control jitter. This result is shown in Fig. 17(a). A comparison between Figs. 16 and 17 shows that the proposed jitter compensator successfully suppresses the control jitter disturbance at low frequencies, and thus most of the regulation error contributed by control jitter is eliminated.

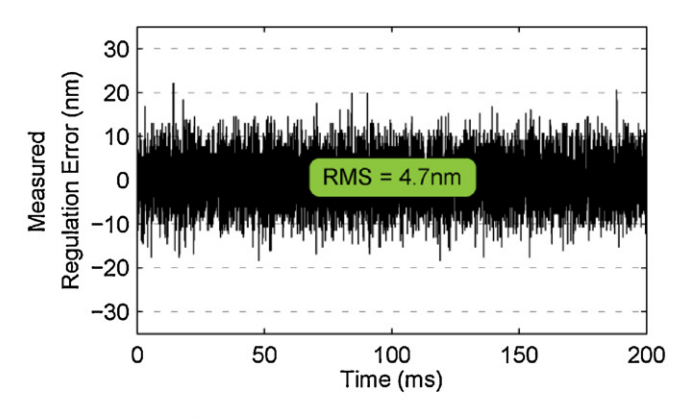
The control jitter regulation error results are extended in Fig. 18, which compares the analytical and measured RMS regulation error for control jitter ranging from 0% to 10% RMS, with and without the jitter compensator implemented. The analytical prediction matches the experiment results very well and the jitter compensator significantly attenuates the effect of control jitter on regulation error.

4.3. Tracking error experimental results for a single harmonic reference command

For the tracking error experiment there is no added measurement noise, $n_a[k]=0$ \forall k, and the reference command is a 6 kHz sinusoidal signal with a 4 μ m peak-to-valley amplitude: $r[k]=2\sin(2\pi\times6000\times kT_0)$ μ m. Generally, tracking at such a high frequency will result in the dominant tracking error contribution coming from the reference command component $\varepsilon_r[k]$, as expressed in Eq. (56). In order to show the tracking error contributed by jitter, $\varepsilon_r[k]$ should be eliminated by increasing the controller gain at 6 kHz to infinity. This can be done by adding an adaptive feed-forward cancelation (AFC) controller [29]

$$C(z) = C_B(z)(1 + C_{AFC}(z)).$$
 (58)

Here, $C_{AFC}(z)$ contains four compensated frequencies at 6 kHz, 12 kHz, 18 kHz, and 24 kHz, each with a gain of 200. The AFC compensation at higher order harmonics of the reference command is used to attenuate tracking error caused by the non-linearity of the FTS actuator. Fig. 19 shows the tracking experiment results for no jitter, with and without $C_{AFC}(z)$. After implementing the AFC controller, the tracking error was reduced by a factor of nearly 1000, from 1.4 μ m RMS to 1.6 nm RMS, which is close to the measurement noise floor. From the tracking PSD comparison in Fig. 19(c),



(a) Measured regulation error in time domain.

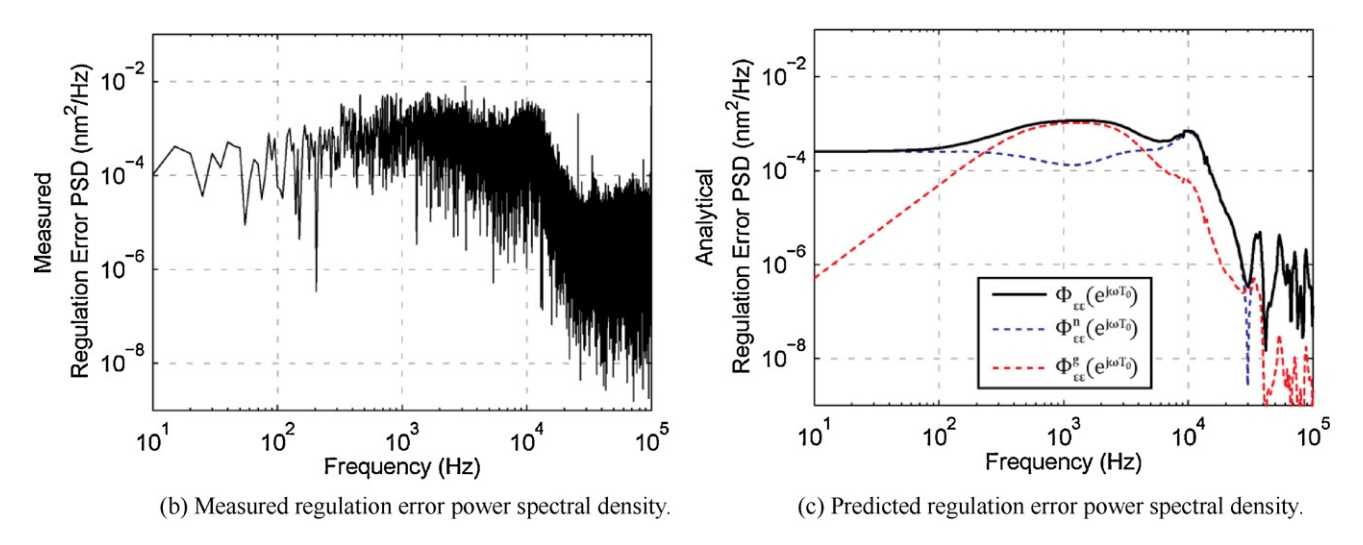


Fig. 17. Regulation error experimental results for 8% control jitter with the jitter compensator included in controller.

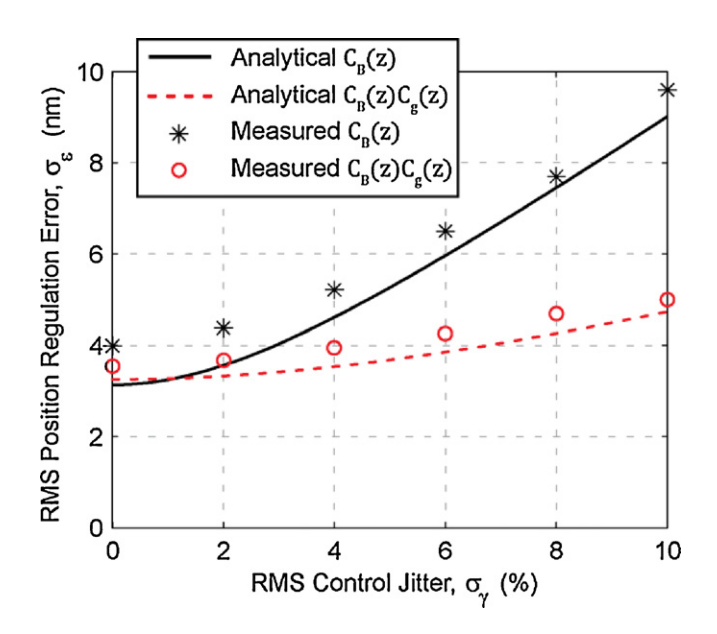
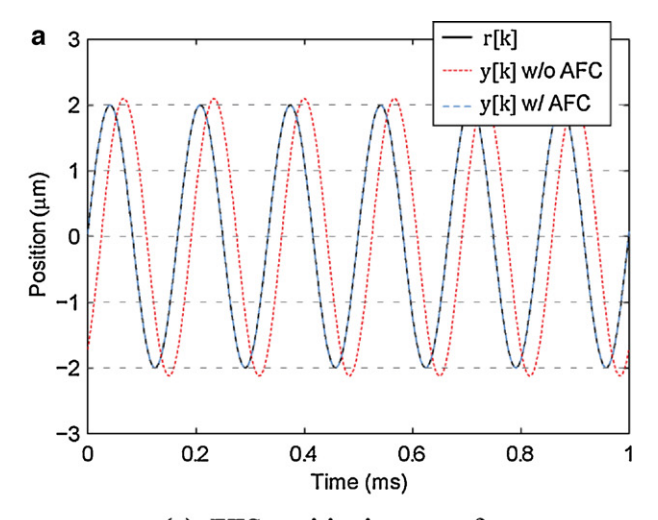


Fig. 18. Measured and analytical RMS regulation error comparison for various amount of control jitter, with and without the jitter compensator.



(a) FTS positioning waveforms.

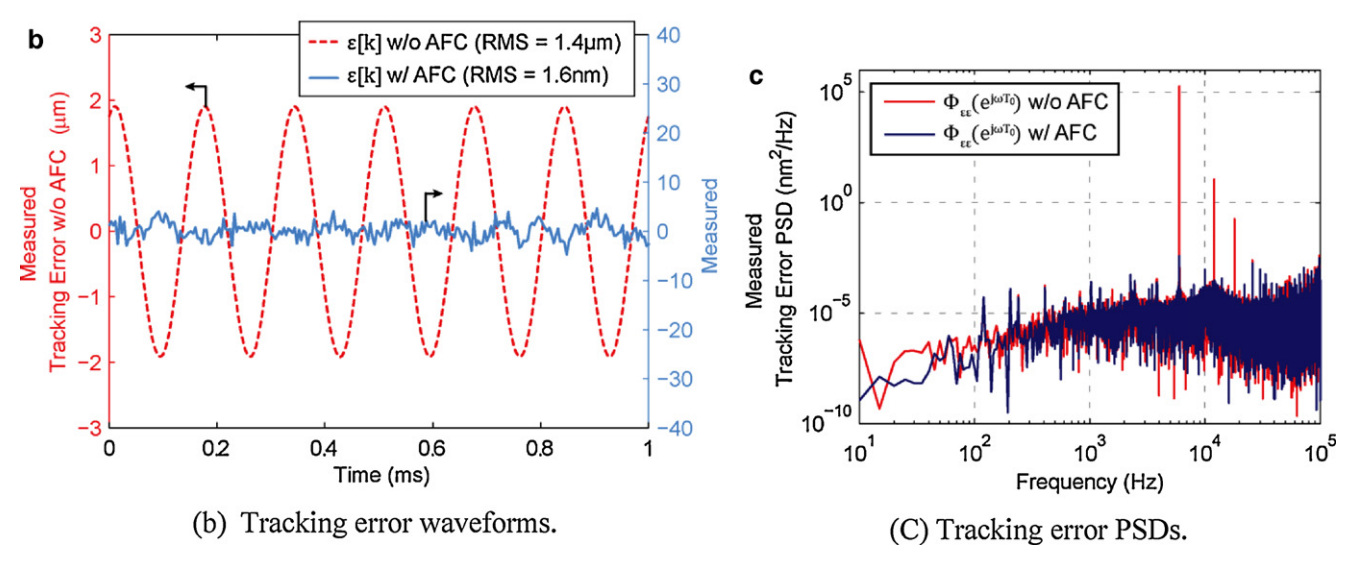


Fig. 19. Tracking error experimental results for no jitter with and without AFC.

the AFC effectively removes all error components at the reference signal frequency as well as at its higher frequency harmonics. In all the following tracking experiments the AFC controller is implemented and the 1.6 nm RMS tracking error with no jitter is used as a benchmark.

4.3.1. Effect of sampling jitter on tracking error

In this experiment the control jitter is set at zero and the sampling jitter is varied from 0% to 10% of the sampling period using the jitter data from Fig. 10. Fig. 20 shows the experimental measured tracking error and its PSD for 8% RMS sampling

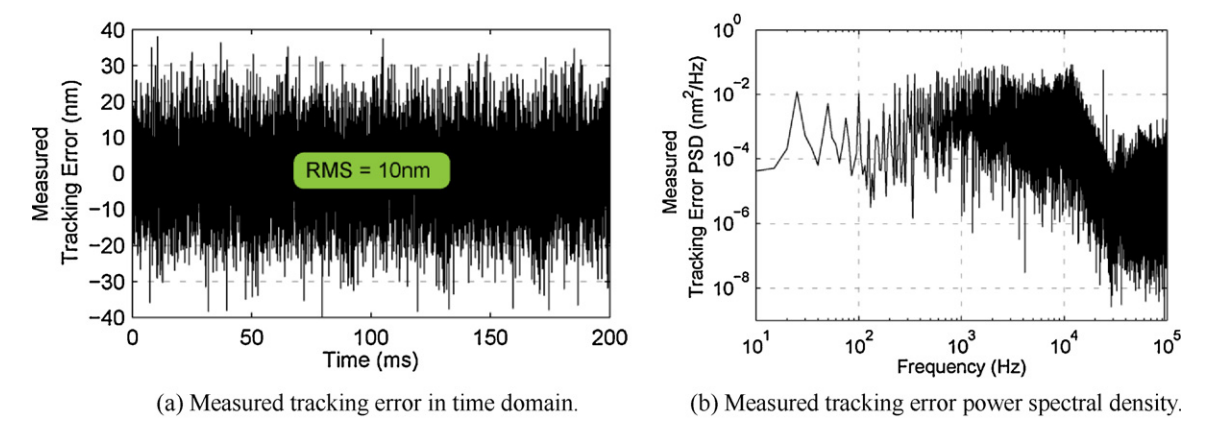
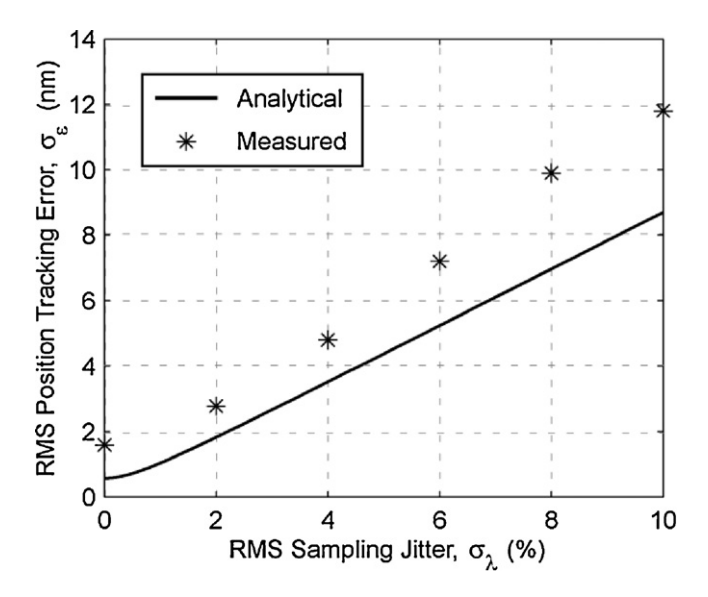
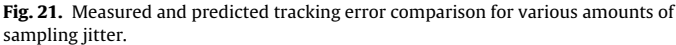


Fig. 20. Tracking error experimental results for 8% sampling jitter.





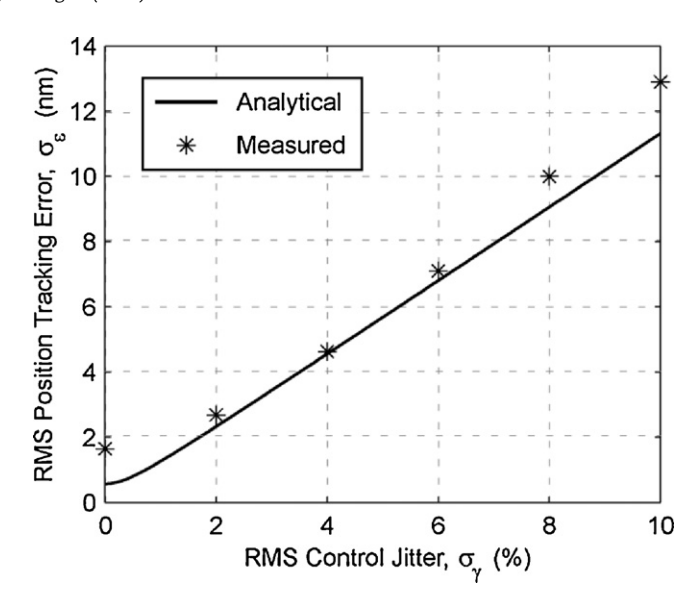


Fig. 23. Measured and predicted tracking error comparison for various amounts of control jitter.

jitter. In comparison with the zero sampling jitter benchmark results in Fig. 19, the tracking error RMS value increased by 6 times, from 1.6 nm to 10 nm. From the tracking error PSD in Fig. 20(b) it can be seen that the major increase in tracking error from sampling jitter occurs in the low frequency region.

The tracking error results with various amounts of sampling jitter are shown in Fig. 21, which compares the analytical RMS tracking error, calculated from Eq. (55), to the experimentally measured RMS tracking error for sampling jitter ranging from 0% to 10%. Notice that as sampling jitter approaches zero, the measured error approaches 1.6 nm RMS, nearly the measurement noise floor for the FTS system. In all cases, the analytical results predict the trend of the experimental results with a small amount of mismatch. This is believed to be related to the FTS plant non-linearity which was not modeled in Fig. 7 and included in the analysis of Eq. (55). These experimental results also indicate that the sampling jitter disturbance h[k] can become the dominant source of positioning error, particularly for high-bandwidth precision motion control systems.

4.3.2. Effect of control jitter on tracking error

In this experiment the sampling jitter is set at zero and the control jitter is varied from 0% to 10% of the sampling period using the jitter data from Fig. 10. Fig. 22 shows the experimental measured tracking error and its PSD with 8% RMS control jitter. In comparison with the zero control jitter benchmark results in Fig. 19, the tracking error RMS increased by 6 times, from 1.6 nm to 9.9 nm. From the tracking error PSD in Fig. 22(b) it can be seen that the major increase in tracking error due to control jitter occurs in the low frequency region, particularly in the frequency range 100 Hz–10 kHz where the controller's disturbance rejection is lowest.

Fig. 23 extends the tracking error results for control jitter, comparing the analytically predicted RMS tracking error, calculated from Eq. (51), to the experimentally measured RMS tracking error for control jitter ranging from 0% to 10%. In all cases the results match very well, validating the presented models and analytical results for control jitter. In addition, the experimental results also demonstrate that control jitter can significantly degrade positioning performance, particularly for high-speed precision motion control systems.

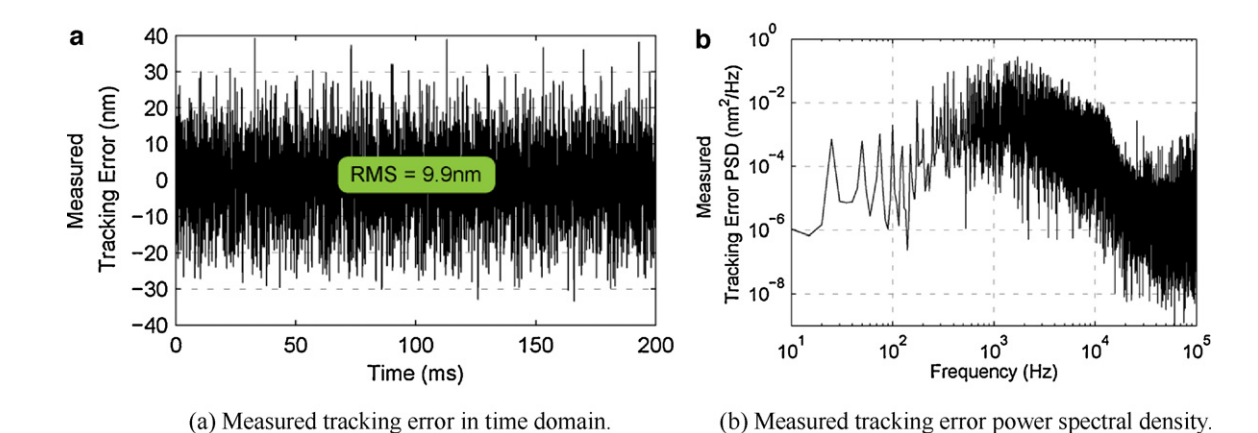
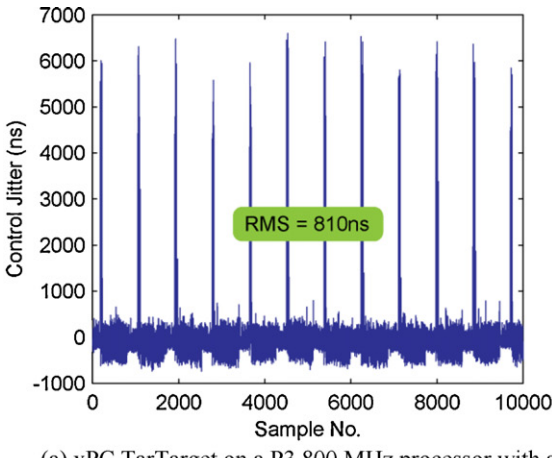
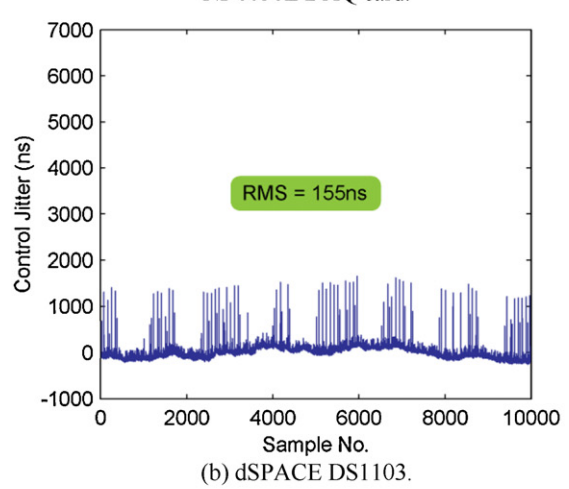


Fig. 22. Tracking error experimental results for 8% control jitter.



(a) xPC TarTarget on a P3 800 MHz processor with a NI-6036E DAO card.



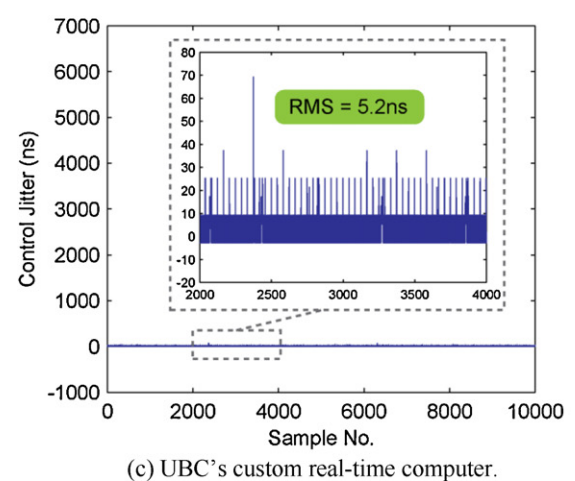


Fig. 24. Control jitter measurements for various Real-Time computers.

5. Conclusions

A new simplified discrete model (Fig. 7) was developed that incorporates the effect of sampling jitter and control jitter as disturbances to the control system. Using this simplified model, analytical formulas (Eqs. (41), (51) and (55)) are derived to predict jitter's effect on positioning error for both regulation and tracking scenarios. These analytical relations, which can be solved using either measured or analytical frequency responses of a control system, are then experimentally demonstrated on a fast-tool servo machine tool.

In the case of position regulation, sampling jitter generally has a negligible effect on positioning error. In comparison, control jitter can significantly degrade regulation performance, with positioning error increasing from 4.0 nm RMS at zero control jitter to 7.7 nm RMS at 8% control jitter in the experiments performed. Adding a simple jitter compensator to the existing motion controller, consisting of a zero at the Nyquist frequency, is shown to greatly mitigate the position regulation error contributed by control jitter, reducing the error to 4.7 nm RMS despite the presence of 8% control jitter.

In the case of position tracking, both sampling jitter and control jitter can significantly increase positioning error. When tracking a $4\,\mu m$ peak-to-valley 6 kHz sinusoidal signal with the fast-tool servo, sampling jitter increased the tracking error from 1.6 nm RMS at zero jitter to 10 nm RMS at 8% jitter. Similarly, control jitter also increased the tracking error to 10 nm RMS at 8% jitter. To attenuate this additional tracking error, either the controller disturbance rejection should be increased via controller redesign or a better control system (hardware and operating system) with less jitter should be utilized.

The close match between the analytical results and the experimental results confirmed that the presented model and analysis can be used to predict jitters' effect on motion control performance, and this is useful to do error budget in motion control system design process.

Appendix A. Jitter measurement

Sampling jitter and control jitter can vary greatly in different real-time computer implementations. It is mainly affected by factors such as task scheduling, input–output device synchronization, interrupt handling, cache misses, and resource sharing.

The simplest way to measure sampling jitter and control jitter is with an input timestamp and output timestamp, respectively; however, many real-time control implementations do not provide this data. Further, even if timestamps are available, their definition and exact implementation can vary from system to system, providing misleading results. To guarantee a fair comparison between different controller implementation, an external time-stamping setup is used here to capture control jitter. The control jitter measurement setup introduces an additional function at the end of a conventional control cycle that switches a secondary DAC output between 0 V and 2.5 V. This output is then sent through a comparator and into an FPGA, which captures the signal edges with 5 ns resolution and stores the control output update timestamps TS[k]. To extract the control jitter from these timestamps TS[k], a least square linear fitting is performed to minimize the following sum

$$\sum_{k} (TS[k] - Ak + B)^2, \tag{59}$$

where A and B are the least squares fitting coefficients and k is the control cycle index. The control jitter is then calculated as

$$\tau_{c}[k] = TS[k] - Ak - B. \tag{60}$$

Control jitter measurements are made for the following three controller implementations:

- xPC Target on a P3 800 MHz processor with a NI-6036E DAQ card;
- dSPACE 1103;
- UBC's custom control platform [28].

As shown by Fig. 24, the xPC Target implementation has 810 ns RMS of control jitter, the dSPACE 1103 implementation has 155 ns RMS of control jitter, and the custom UBC platform has 5.2 ns RMS of control jitter. While there are some deterministic components

to the control jitter, most of the signal energy comes from the white random component. These results clearly demonstrate how greatly control jitter can vary depending on the real-time computing hardware. Other general purpose platforms exhibit several microseconds of jitter [8,9].

Appendix B. Tracking error analysis for non-repetitive reference command

Repetitive command tracking error is analyzed in Section 3.2. Here only non-repetitive finite-energy reference command is considered, as non-repetitive infinite-energy gives infinite-energy error. When a non-repetitive reference command has finite energy $\sum_{k=-\infty}^{\infty} r^2[k] < \infty$, its Fourier transform exists and can be expressed as

$$R(e^{j\Omega}) = \sum_{k=-\infty}^{\infty} r[k]e^{-jk\Omega}.$$
(61)

The total summed square of $\varepsilon_r[k]$ is calculated as from the discrete model in Fig. 7

$$\sum_{k=-\infty}^{\infty} \varepsilon_r^2[k] = \frac{1}{2\pi} \int_{-\pi}^{\pi} \left| \frac{R(e^{j\Omega})}{1 + P_z(e^{j\Omega})C(e^{j\Omega})} \right|^2 d\Omega.$$
 (62)

Although $\varepsilon_g[k]$'s variance is time-varying, the summed variance of $\varepsilon_g[k]$ can be derived as follows:

$$\sum_{k=-\infty}^{\infty} E(\varepsilon_g^2[k]) = \sum_{k=-\infty}^{\infty} E(g^2[k]) \frac{1}{2\pi} \int_{-\pi}^{\pi} \left| \frac{P_z(e^{j\Omega})}{1 + P_z(e^{j\Omega})C(e^{j\Omega})} \right|^2 d\Omega$$

$$=\sigma_{\gamma}^{2} \sum_{k=-\infty}^{\infty} u_{\Delta}^{2}[k] \frac{1}{2\pi} \int_{-\pi}^{\pi} \left| \frac{P_{z}(e^{j\Omega})}{1 + P_{z}(e^{j\Omega})C(e^{j\Omega})} \right|^{2} d\Omega.$$
 (63)

According to Parseval's identity [30]

$$\sum_{k=-\infty}^{\infty} u_{\Delta}^{2}[k] = \frac{1}{2\pi} \int_{-\pi}^{\pi} \left| \frac{R(e^{j\Omega})C(e^{j\Omega})(e^{-j\Omega} - 1)}{1 + P_{z}(e^{j\Omega})C(e^{j\Omega})} \right|^{2} d\Omega.$$
 (64)

As a result, the summed variance of $\varepsilon_g[k]$ is

$$\sum_{k=-\infty}^{\infty} E(\varepsilon_g^2[k]) = \sigma_{\gamma}^2 \left(\frac{1}{2\pi} \int_{-\pi}^{\pi} \left| \frac{R(e^{j\Omega})C(e^{j\Omega})(e^{-j\Omega} - 1)}{1 + P_z(e^{j\Omega})C(e^{j\Omega})} \right|^2 d\Omega \right) \times \left(\frac{1}{2\pi} \int_{-\pi}^{\pi} \left| \frac{P_z(e^{j\Omega})}{1 + P_z(e^{j\Omega})C(e^{j\Omega})} \right|^2 d\Omega \right).$$
 (65)

Similarly, the summed variance of $\varepsilon_h[k]$ for non-repetitive reference command is derived as

$$\sum_{k=-\infty}^{\infty} E(\varepsilon_{h}^{2}[k]) = \sum_{k=-\infty}^{\infty} E(h^{2}[k]) \frac{1}{2\pi} \int_{-\pi}^{\pi} \left| \frac{P_{z}(e^{j\Omega})C(e^{j\Omega})}{1 + P_{z}(e^{j\Omega})C(e^{j\Omega})} \right|^{2} d\Omega$$

$$= \sigma_{\lambda}^{2} \sum_{k=-\infty}^{\infty} y_{\Delta}^{2}[k] \frac{1}{2\pi} \int_{-\pi}^{\pi} \left| \frac{P_{z}(e^{j\Omega})C(e^{j\Omega})}{1 + P_{z}(e^{j\Omega})C(e^{j\Omega})} \right|^{2} d\Omega$$

$$= \sigma_{\lambda}^{2} \left(\frac{1}{2\pi} \int_{-\pi}^{\pi} \left| \frac{R(e^{j\Omega})P_{z}(e^{j\Omega})C(e^{j\Omega})(1 - e^{-j\Omega})}{1 + P_{z}(e^{j\Omega})C(e^{j\Omega})} \right|^{2} d\Omega \right)$$

$$\times \left(\frac{1}{2\pi} \int_{-\pi}^{\pi} \left| \frac{P_{z}(e^{j\Omega})C(e^{j\Omega})}{1 + P_{z}(e^{j\Omega})C(e^{j\Omega})} \right|^{2} d\Omega \right). \tag{66}$$

References

- [1] Åström K, Wittenmark B. Computer-controlled systems: theory and design. 3rd ed. Prentice Hall; 1997.
- [2] Franklin G, Powell J, Workman M. Digital control of dynamic systems, 3rd ed. Addison-Wesley; 1998.
- [3] Wittenmark B, Nilsson J, Torngren M. Timing problems in real-time control systems. In: Proceedings of the 1995 American control conference, vol. 3. 1995. p. 2000–4.
- [4] Kushner H, Tobias L. On the stability of randomly sampled systems. IEEE Transactions on Automatic Control 1969;14:319–24.
- [5] Cao Y-Y, Sun Y-X, Cheng C. Delay-dependent robust stabilization of uncertain systems with multiple state delays. IEEE Transactions on Automatic Control 1998:43:1608–12.
- [6] Fridman E, Shaked U. Delay-dependent stability and H∞ control: constant and time-varying delays. International Journal of Control 2003;76: 48–60.
- [7] Kao C-Y, Lincoln B. Simple stability criteria for systems with time-varying delays. Automatica 2004;40:1429–34.
- [8] Proctor F, Shackleford W. Real-time operating system timing jitter and its impact on motor control. Society of Photo-Optical Instrumentation Engineers (SPIE) Conference Series 2001;4563:10–6.
- [9] Rosol M, Pilat A, Turnau A. Real-time controller design based on NI Compact-RIO. In: Proceedings of the international multiconference on computer science and information technology. 2010. p. 825–30.
- [10] Ohlin M, Henriksson D, Cervin A. TrueTime 1.5-reference manual. Sweden: Department of Automatic Control, Lund University; 2007.
- [11] Cervin A, Lincoln B. Jitterbug 1.1-reference manual. Sweden: Department of Automatic Control, Lund Institute of Technology; 2003.
- [12] Cervin A, Henriksson D, Lincoln B, Eker J, Arzen K-E. How does control timing affect performance? Analysis and simulation of timing using Jitterbug and TrueTime. IEEE Control Systems Magazine 2003;23:16–30.
- [13] Antunes A, Mota A. Control performance of a real-time adaptive distributed control system under jitter conditions. In: Proceedings of control 2004 conference, 2004.
- [14] Zhang C, Li D, Ye F, Lai Y, Wan J. Modeling of computer-controlled systems with sampling interval jitter. In: Proceedings of the 2010 international conference on measuring technology and mechatronics automation, vol. 2. IEEE Computer Society; 2010. p. 683–6.
- [15] Kobayashi Y, Kimura T, Fujioka H. A servo motor control with sampling jitters. In: IEEE 11th international workshop on advanced motion control. 2010. p. 58-63
- [16] Boje E. Approximate models for continuous-time linear systems with sampling jitter. Automatica 2005;41:2091–8.
- [17] Crespo A, Ripoll I, Albertos P. Reducing delays in RT control: the control action interval. In: Proceedings of the IFAC world congress. 1999.
- [18] Tian Y-C, Han Q-L, Levy D, Tade M. Reducing control latency and jitter in realtime control. Asian Journal of Control 2006;8:72–5.
- [19] Buttazzo G, Cervin A. Comparative assessment and evaluation of jitter control methods. In: Proceedings of the 15th international conference on real-time and network systems. 2007.
- [20] Lozoya C, Velasco M, Marti P. The one-shot task model for robust realtime embedded control systems. IEEE Transactions on Industrial Informatics 2008;4:164–74.
- [21] Nilsson J, Bernhardsson B, Wittenmark B. Stochastic analysis and control of real-time systems with random time delays. Automatica 1998;34: 57–64.
- [22] Suplin V, Fridman E, Shaked U. Sampled-data H[infinity] control and filtering: nonuniform uncertain sampling. Automatica 2007;43: 1072–83.
- [23] Marti P, Fuertes J, Fohler G, Ramamritham K. Jitter compensation for real-time control systems. In: Proceedings of the IEEE real-time systems symposium. 2001. p. 39–48.
- [24] Lincoln B. Jitter compensation in digital control systems. In: Proceedings of the 2002 American control conference, vol. 4, 2002. p. 2985–90.
- [25] Niculae D, Plaisanu C, Bistriceanu D. Sampling jitter compensation for numeric PID controllers. In: IEEE international conference on automation, quality and testing, robotics, vol. 2. 2008. p. 100–4.
- [26] Oppenheim A, Schafer R, Buck J. Discrete-time signal processing. 2nd ed. Prentice Hall: 1999.
- [27] Lu X-D, Trumper D. Ultrafast tool servos for diamond turning. CIRP Annals Manufacturing Technology 2005;54:383–8.
- [28] Smeds K, Lu X-D. A multirate multiprocessor control platform for high-speed precision motion control. In: Proceedings of the ASPE 25th annual meeting. 2010.
- [29] Lu X-D, Trumper D. High bandwidth fast tool servo control. In: Proceedings of the 2004 American control conference, vol. 1. 2004.
- [30] Oppenheim A, Willsky A, Nawab S. Signals and systems. Prentice Hall; 1997.